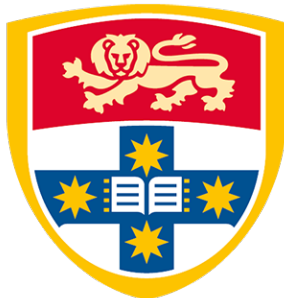


Development of a Low Cost Flowmeter for Neonatal Respiratory Monitoring



THE UNIVERSITY OF
SYDNEY

AUTHOR

Jack Hall

STUDENT ID :

470413537

Supervisor

Prof. Alistair McEwan

Abstract

Evidence suggests that Respiratory Function Monitors improve resuscitation by displaying key parameters to practitioners at the time of birth. Current devices however, are excessively bulky and expensive. With 99% of neonatal deaths occurring in low-resource settings, drastic interventions are required to tailor existing technology to realistically engage the most effected domains. This thesis developed a fixed orifice flow meter that exhibits the range and sensitivity ideal to monitor neonatal resuscitation. The prototype uses low-cost materials, with a final price of <\$40AUD. Four elements of 2.5, 3, 3.5 and 4 mm constrictions underwent experimental assessment; investigating their sensitivity, bidirectionality, accuracy and pneumatic resistance. Results precipitated a judgement that the 4mm orifice would best suit the needs of an asphyxiated infant. A summary of the prevailing characteristics of each flow element is as below:

Size (mm)	Max Flow (slm)	Average Sensitivity (Pa/L·min ⁻¹)	Dead Space (mL)	Peak Resistance (Pa)
2.5	7.43	64.92	1.37	207.60
3.0	11.85	73.21	1.38	223.98
3.5	16.82	31.56	1.39	197.24
4.0	24.24	14.87	1.40	170.99

Table 1: Summary of the Key Results Characterising Each Pneumotachograph

Acknowledgments

This thesis would not exist without the incredible work that has been done by the entire team at ResusRight. Your dedication to saving lives is consistently inspiring. I would like to extend a specific thanks to Matthew Crott, your guidance from start to finish has been invaluable. To my supervisor, Prof. Alistair McEwan, thank you for extending your knowledge throughout this project.

Finally, I would like to thank my Mum, Dad, Sisters and friends for all you do to love and support me.

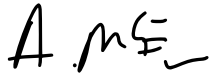
Statement of Contributions

- I shaped the aims of this thesis with Matthew Crott of ResusRight.
- I carried out the review of the literature.
- I assessed commercially available components to land on those that would best suit the overall system.
- I wrote the code to connect the sensor (SDP31) to the microcontroller (ESP32).
- I designed the flow elements in Computer Aided Design (CAD).
- I printed and processed each 3D print.
- I set up and performed the Computational Fluid Dynamics Simulation.
- I performed all experimentation outlined within this thesis.
- I processed all data and plotted results through MATLAB software.
- I assessed and concluded on the results from experimentation.

The above represents an accurate summary of the student's contribution.



Jack Hall



Prof. Alistair McEwan

Contents

Abstract	1
Acknowledgments	2
1 Introduction	9
1.1 Motivation	9
1.2 Clinical Need for Respiratory Function Monitors	10
1.3 Thesis Objectives	12
2 Literature Review	13
2.1 Transitioning from Intrauterine to Extrauterine Life	13
2.1.1 Liquid Clearance and Lung Aeration	14
2.2 Variables Influencing Resuscitation	17
2.3 Respiratory Function Monitors	19
2.4 Technical Operation	20
2.5 Hot Wire Anemometers	22
2.6 Pneumotachometers	24
2.6.1 Non-Linear Pneumotachographs	24
2.6.2 Linear Pneumotachographs	25
2.6.3 Constraints in Designing a Pneumotachometer	26
2.7 Commercially Available Devices	27
3 Commercial Considerations	28
4 Methodology	30
4.1 Selection of the Differential Pressure Sensor	31

CONTENTS

4.2 Computational Unit	33
4.3 Design of the Flow Element	34
4.3.1 Constraints	34
4.3.2 Early Prototypes	34
4.4 Manufacturing and Assembly	36
4.5 Preliminary Validation	37
4.6 Improvements	38
4.7 Testing	41
4.7.1 Calibration of the Flow Sensors	41
4.7.2 Assessment of Flow Rate Error	43
4.7.3 Performance Validation	43
4.7.4 Computational Fluid Dynamics: Testing Resistance	44
5 Results	45
5.1 Calibration Curves	45
5.2 Experimental Outcome vs Analytic Prediction	48
5.3 Assessment of Bidirectional Behaviour	50
5.4 Assessment of Flow Rate Error	51
5.5 Performance Validation	52
5.6 Computational Fluid Dynamics	54
6 Discussion	56
6.1 Selection of the Best Pneumotachograph	58
6.2 Measurement Error	59
6.3 Error in Experimental Setup	63
6.4 Cost	64
6.5 Conclusion and Future Work	65
A	79
A.1 Test conditions for ventilatory performance: ISO 10651-4:2009	79
A.2 Interconnecting details of cones and sockets: ISO 5356-1:2015(E)	80

A.3 Raw Signal From Experiment 4.7.1	81
A.4 Image of the Test Setup for 4.7.3	82

List of Figures

1.1 Diagram of a typical SIB and Mask	10
1.2 RFM Display	11
2.1 Lung Volumes and Parameters	14
2.2 Phase Contrast X-ray images from Hooper et al. demonstrating gas volumes from birth in spontaneously breathing newborn rabbit pup	15
2.3 Phase contrast X-ray of dead rabbit pups under mechanical ventilation	16
2.4 PPV as determined by pressure settings, mask technique and newborn phys- iology	18
2.5 New Life Box (Advanced Life Diagnostics) RFM used in a clinical trial of Respiratory Rate Postnatal	20
2.6 Respiratory rate (RR) to maintain normocapnia (40 mmHg) when varying apparatus dead space and patient weight	21
2.7 Development of sensing bi-directional flow in Hot Wire Anemometers from the 3-wire method to a hot body in silicon	23
2.8 Venturi Type Pneumotacograph	24
2.9 Comparision between Lilly and Fleisch type pneumotachographs	25
3.1 Juno Training Monitor (ResusRight)	28
3.2 SFM3400 Flow Sensor (Sensirion)	29
4.1 Flow Sensing System Overview	31
4.2 Calibration Curve BREATHNEY Sensor Module	32
4.3 Calibration Curve For Neonatal Flow Sensor Assessed by Schena et al.	33

LIST OF FIGURES

4.4 Venturi Like Design for Early Prototype	35
4.5 3D-printed Flow Elements After Curing for 60 minutes at 70°C	36
4.6 Simulated Infant Breath Signal Prototype 1	37
4.7 Fixed Orifice Pneumotachograph (3.5mm)	38
4.8 Full Integration of the Flow Sensor Attached to a Self Inflating Bag and Standalone	39
4.9 Analytical Estimate of Maximum Flow by Orifice Diameter	40
4.10 Experimental Setup: Differential Pressure vs Flow	42
4.11 Experimental Setup for Performance Validation Testing	43
5.1 Calibration Curve for 2.5, 3, 3.5 and 4mm Fixed Orifice Pneumotachographs	45
5.2 Sensitivity assessed by Low, Medium and High Flow Ranges	46
5.3 How Maximum Sensed Flow and Sensitivity Varied with Orifice Size	47
5.4 Calibration Curves Plotted with Their Theoretical Estimate	48
5.5 Analysis of Symmetry Between Inspiratory and Expiratory Flow for Each Orifice Size	50
5.6 Flow Error of Prototypes Against the Control. Ranges are Split into Low (0-5 slm) Medium (5-10 slm) and High (10-15 slm) Flow	51
5.7 Wave-forms of 4mm Orifice Under Test Lung Simulation	52
5.8 Wave-forms for all Prototypes Under Test Lung Simulation	53
5.9 Computational Fluid Dynamics: Static Pressure at 5L/min (2.5mm)	54
5.10 Computational Fluid Dynamics: Static Pressure at 5L/min (3.5mm)	54
5.11 Computational Fluid Dynamics: Velocity Magnitude (3.5mm)	55
6.1 Error Against Measured Flow in a Low Cost Flow Sensor Designed by Ed- munds et al.	57
6.2 Calibration curve at low flows (0-5slm)	59
6.3 3D-Printing Defects	61
6.4 Calibration of the flow sensor for the Princeton Open Ventilation Monitor with Observed Defects	62
6.5 a. before and b. after frozen CO2 deburring	62

6.6 Calibration of the flow sensor for the Princeton Open Ventilation Monitor	63
A.1 BS EN ISO 10651-4:2009h	79
A.2 Dimensions of cones and sockets	80
A.3 Raw Signals: Differential Pressure vs Flow for 3.5mm Orifice	81
A.4 Experimental Setup for Test 4.7.3	82

List of Tables

1 Summary of the Key Results Characterising Each Pneumotachograph	1
5.1 Calibration Results: Maximum Sensed Flow and Sensitivity by Orifice Size	46
5.2 Difference between Observed and Predicted Maximum Sensed Flow	47
5.3 Summary of RMSE Between Predicted and Experimentally Fit Curves	49
5.4 Summary of Dead Space and Peak Pneumatic Resistance for Each Prototype	55
6.1 Cost Summary	64

Chapter 1

Introduction

1.1 Motivation

Globally, 165 million infants are born every year, of which over 10 million require resuscitation and 1 million die from intrapartum-related complications [1]. Overall, 99% of these deaths occur in resource-poor settings [2]. Staggeringly, Wall et al suggest that 30% of asphyxiated deaths may have been prevented by adequate neonatal resuscitation training at the facility level [3]. Moreover, these statistics do not encapsulate survivors who are burdened with life-long pathologies, either from insufficient ventilation and hypoxic-ischaemic organ damage, or excessive ventilation and barotrauma to the immature lung [4]. As a consequence, child-hood survivors of perinatal asphyxia may adopt a variety of visual, auditory, and intellectual impairments. A recent meta-analysis by Zhang et al. found that 17.3% of asphyxiated neonates presenting with hypoxic ischemic encephalopathy developed Cerebral Palsy [5]. Unfortunately, in developing countries, accurate epidemiological data is scarce, with estimates for neurodevelopmental sequelae from birth asphyxia still readily debated [6][7][8]. Studies in developed countries have found that approximately 18% of infants who suffer moderate to severe asphyxia are disabled by 8 years of age [9].

1.2 Clinical Need for Respiratory Function Monitors

The neonatal transition from in utero oxygenation to pulmonary gas exchange is arguably the most complex physiological adaptation humans undergo. As a result of such complexity, the stabilisation and resuscitation of babies at birth is one of the most frequently performed procedures, with Positive Pressure Ventilation (PPV) the cornerstone in clinical settings [10]. Current guidelines suggest that if apnoea is combined with bradycardia (heart rate < 100 bpm) at birth, PPV must be administered [11].

Devices used to administer PPV can be classified into those that are flow generating, seen in the self inflating bag (SIB), or flow dependent, as in the flow inflating bag and t-piece resuscitator. The SIB is the only one that does not require a fresh gas supply and is therefore the most widely adopted [12]. A recent world health initiative has seen a push for the provision of SIBs to all birth attendants in low-income and middle-income countries. The United Nations commission on Life-Saving Commodities for Women and Children, and the World Health Organisation (WHO), recently listed the SIB as a critical medical technology in reducing intrapartum deaths globally [13] [14].

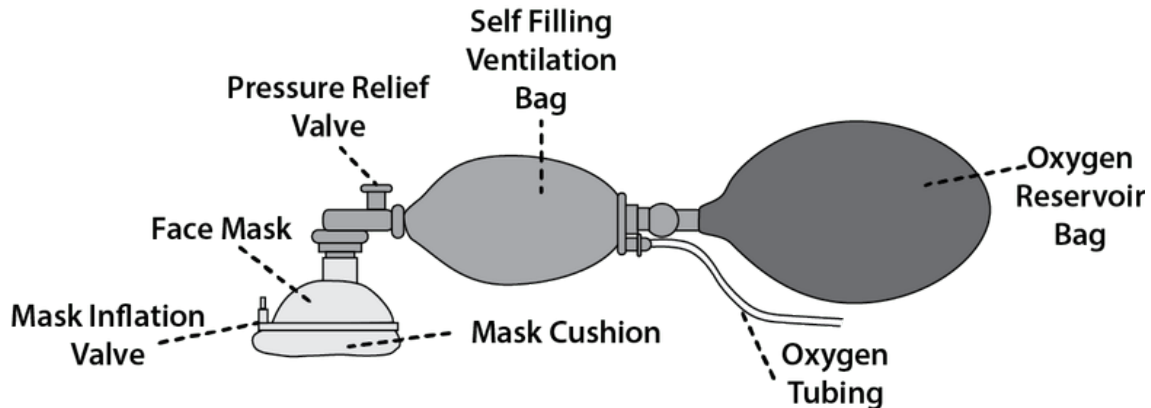


Figure 1.1: Diagram of a typical SIB and Mask [15]

In spite of the therapeutic strength of SIBs and their widespread adoption, many suggest that most do not adequately meet required standards [16] [17] or that standards are too low [12]. Tracey et al. performed a bench-top test of 20 models of SIB, incrementally compressed

by a robotic device, to assess their ability to titrate an appropriate tidal volume and peak pressure [17]. Ten out of the twenty devices failed their testing with researchers concluding that “the consequence of this poor performance may not be observable by the operator and stated compliance with international standards for SIB (≤ 5 kgs) does not guarantee safety and efficacy of delivered ventilation”. In addition to hardware failure, many suggest basic user technique is at fault in the deliverance of inadequate ventilation. Observing 100 resuscitation’s, Carbine et al. found 54 significantly deviated from recommended guidelines [18].

The use of a Respiratory Function Monitor (RFM) has been investigated as a response to pitfalls in mechanical ventilation. The technology employs a graphical display to assess mask leak (leakage at the interface with the patient), tidal volume (V_T) and Peak Inspiratory Pressure (PIP), among other key parameters of respiratory function.

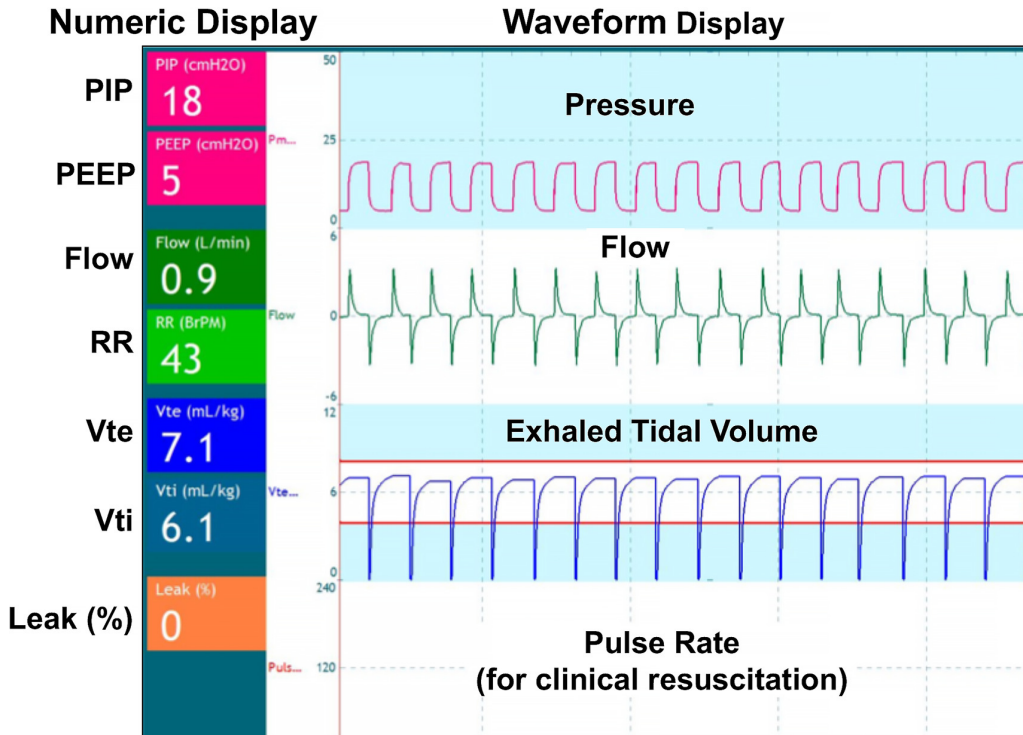


Figure 1.2: RFM Display [19]

Many studies purport a direct clinical response in improving resuscitation overall through the use of a RFM [20][21][22]. A study by Wood et al. found a median reduction in mask leak from 24.3% to 13.1% when 25 participants used a Florian Infant Graphic Monitor (Acutronic Medical Systems) [23].

However successful in literature, their uptake in clinical practice has been limited, with current devices remaining overly expensive or impractical. Lilley et al investigated the use of a respiratory function monitor during neonatal emergency transport, using a Florian monitor to inform care. While researchers commented on the strength of the monitor to positively inform intervention, their review stated limitations in the devices size, weight, and need for a 240V power source [24]. Therefore, reducing the cost and increasing the portability of respiratory function monitors, for their use in low-resource environments, where 99% of neonatal deaths occur, presents a clear strategy in reducing child mortality and morbidity globally.

1.3 Thesis Objectives

This thesis engages the research of low-cost gas flow sensors tuned to the specific constraints of neonatal ventilation. The overall aim of the thesis is to prove the efficacy of using a differential pressure based pneumotachometer to reduce the cost in flow dependent technology. A successful design should occupy a small dead space, be sensitive to minute gas flows, be bidirectional in nature and require minimal resources to manufacture and operate. The origin of these aims was developed in the following literature review, evaluated through design and testing and rigorously assessed in final discussions.

Chapter 2

Literature Review

2.1 Transitioning from Intrauterine to Extrauterine Life

The transition from intrauterine to extrauterine life at birth requires the rapid adaptation of multiple organ systems for the successful conversion from placental to pulmonary gas exchange. Therefore, understanding the interdependency of such successful physiological events can highlight markers for an atypical transition in clinical practice.

The physiology of the fetus is fundamentally different from that of the neonate, with its cardiopulmonary system dependent entirely on the placenta [25]. Our predominant understanding of the circulatory pathways of the fetus were obtained in 1946 by Sir Joseph Barcroft's collations on fetal sheep [26], with recent advances in MRI imaging quantifying these measurements [27]. In review, oxygenated maternal blood is passed to the fetus within the free-flowing placental space; a low resistance vascular bed that ensures deoxygenated blood returns for exchange [28]. Fetal lungs are unused and filled with fluid to facilitate maturation and growth, they represent an area of opposingly high resistance, so most pulmonary flow is diverted through ducts unique to gestation: the foramen ovale and the ductus arteriosus [29]. A healthy baby's first few breaths inflate the lungs, rapidly dropping the resistance they present to the circulatory system, functionally closing the foramen ovale and allowing deoxygenated blood to be exchanged through pulmonary flow [30].

In these first few breaths, the newborn needs to rapidly clear its airways of fetal lung fluid to build up its functional residual capacity (FRC) and generate an appropriate tidal volume (V_T) in order to facilitate sufficient gas exchange [31].

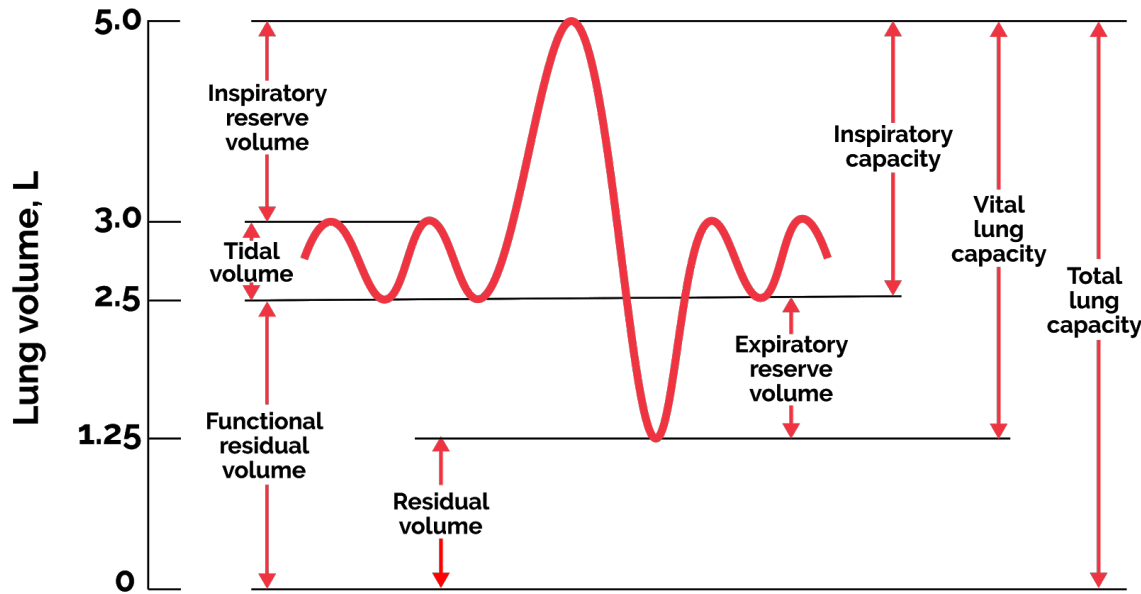


Figure 2.1: Lung Volumes and Parameters [32]

2.1.1 Liquid Clearance and Lung Aeration

As the foetus develops, its airways are filled with fluid secreted by lung epithelium [33]. Whilst the exact volume of liquid in the lung before birth is not agreed upon, evidence indicates that it is greater than any FRC measured post-labour [34]. Large volumes are accumulated through gestation as the glottis restricts its exit, where this over-expansion acts as an essential physiological stimulus for fetal lung development [35].

However, at birth, this liquid must be cleared. Whilst liquid retention is a significant cause of respiratory failure, the literature still readily debates mechanisms for clearance [36] [37]. Mechanisms include mechanical forces imposed on the fetus during labour, as well as the reversal of trans-epithelial gradients from secretion to uptake [38].

Irrespective of the mechanism of fluid clearance through labour, lung fluid remains in the lungs up until the newborns first breath [34]. Spontaneously breathing infants are able to generate an 'opening pressure' from diaphragmatic stimuli and inhalation, to pull the fetal lung fluid from the airways into distal spaces [39]. Functional residual capacity (FRC) is achieved through subsequent breaths as expiratory volumes sit lower than inspiratory. A human observational study by Tepas et al. looked to quantify these patterns, where an RFM was used to analyse the respiratory characteristics of spontaneously breathing infants both at term and preterm [40]. They found that both groups frequently brake their expiration, mostly by crying, to achieve large tidal volumes (6.7 vs 6.5 mL/kg), high peak inspiratory flows (5.7 vs 8.0 L/min) and lower peak expiratory flows (3.6 vs 4.8 L/min). These patterns were also observed in the landmark study by Hooper et al. through phase contrast imaging of fetal rabbits [34].

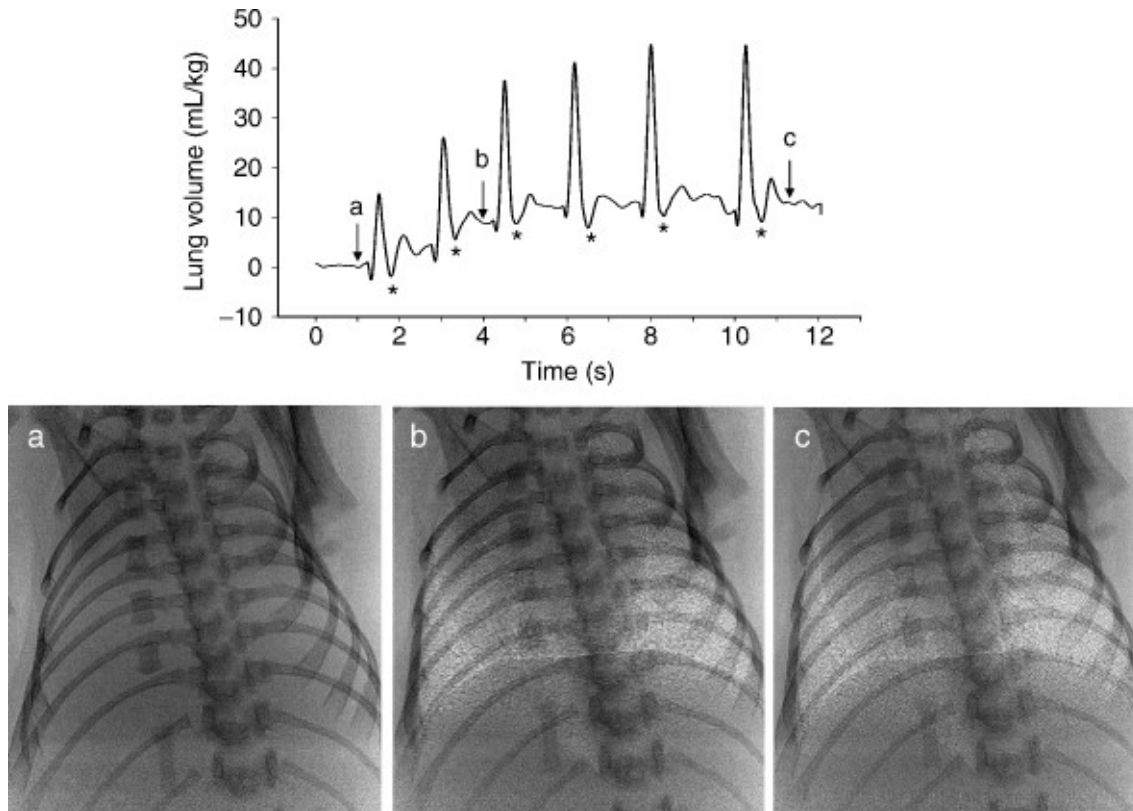


Figure 2.2: Phase Contrast X-ray images from Hooper et al. demonstrating gas volumes from birth in spontaneously breathing newborn rabbit pup [34]

Additionally, in this same study, the researchers established that this trans-pulmonary hydrostatic pressure was the predominant driving force of liquid clearance overall. This conclusion opposed their previous findings [41] and that of the field [33][42], when they observed lung aeration in the ventilation of dead rabbits where labour-induced liquid clearance could not be activated.

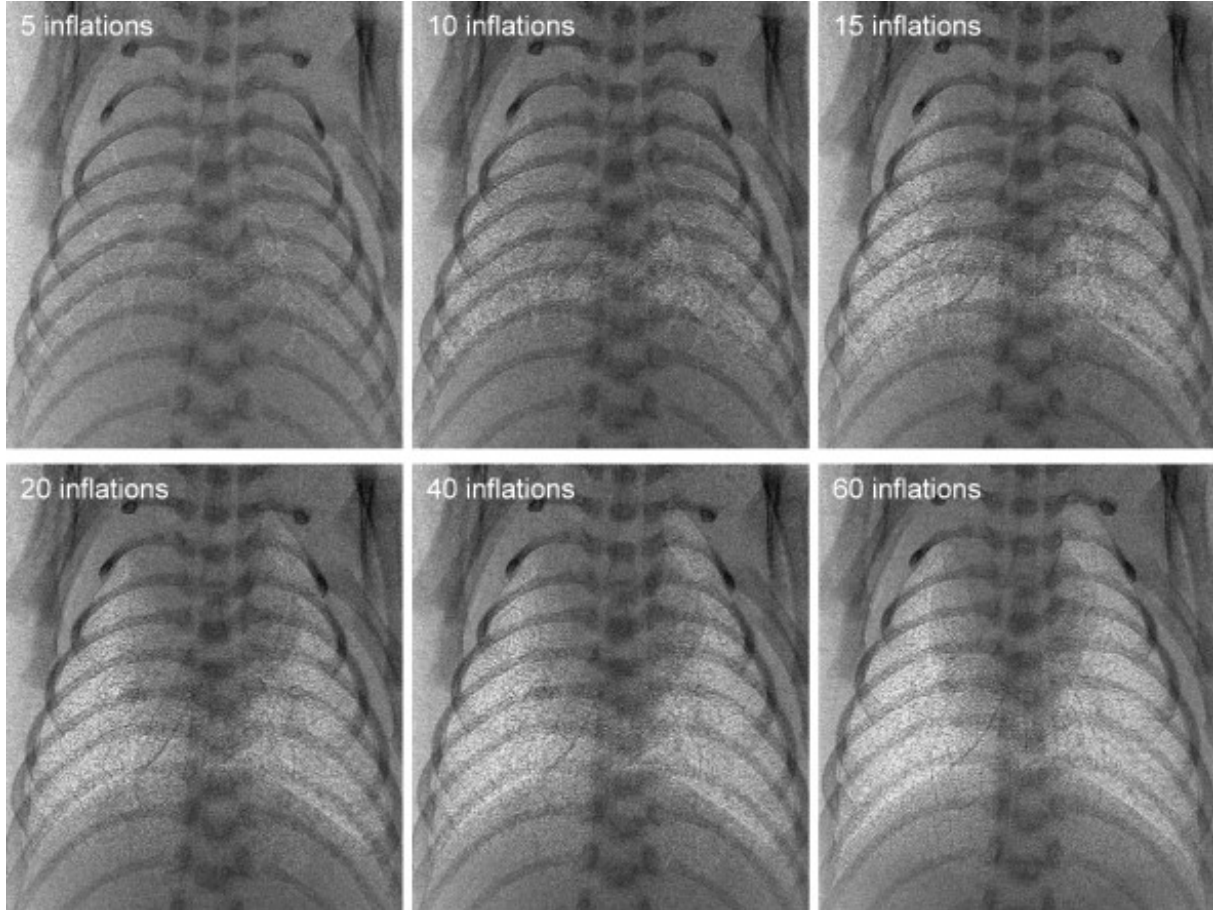


Figure 2.3: Phase contrast X-ray of dead rabbit pups under mechanical ventilation [34]

Therefore, for newly born infants, who cannot generate an adequate transpulmonary pressure, perform spontaneous clearance and aerate on their own, it is clear why PPV is suggested to deliver the hydrostatic pressures necessary to maintain a functional residual capacity.

2.2 Variables Influencing Resuscitation

Many exogenous variables, if unaccounted for at the time of resuscitation, have been shown to contribute to inadequate aeration or injury to the immature lung [4]. Excessive end-expiratory pressures, inadequate or excessive tidal volumes, gas flow rate and the condition of that gas (temperature/humidity) are variables that may fall on a resuscitation team who are very commonly unaware of their contribution.

Standard technique for PPV has long been to regulate delivered volumes by varying the pressure applied to the bag, with Peak Inspiratory Pressure (PIP) generally set at 20 cmH₂O, increasing to 40 cmH₂O depending on the compliance of the infant lung [43]. However, Kattwinkel et al. suggest that resuscitators can be far more responsive to changes in the compliance of a compromised neonate if they can respond to delivered tidal volumes, rather than being guided by prescribed pressure alone [44]. O'Donnell et al. reinforced this assessment in a manikin study, finding PIP as a poor proxy for volumes delivered, contributing this lack of efficacy to its inability to account for mask leak [45]. The mask leak at the interface between a device and the patient can be calculated based on the volumes delivered in inspiration (V_{Ti}) and those returned on expiration (V_{Te}):

$$\text{maskleak} = \frac{V_I - V_E}{V_T} \quad (2.1)$$

A study by Schmolzer et al. in the delivery room, identified a significant mask leak (>75%) in 70% of the 106 resuscitation's they observed [46]. In assessing the impact of mask leak, a review by Martherus et al. aimed to describe its detrimental effect based on its confluence with pressure, tidal volumes and infant physiology [47]:

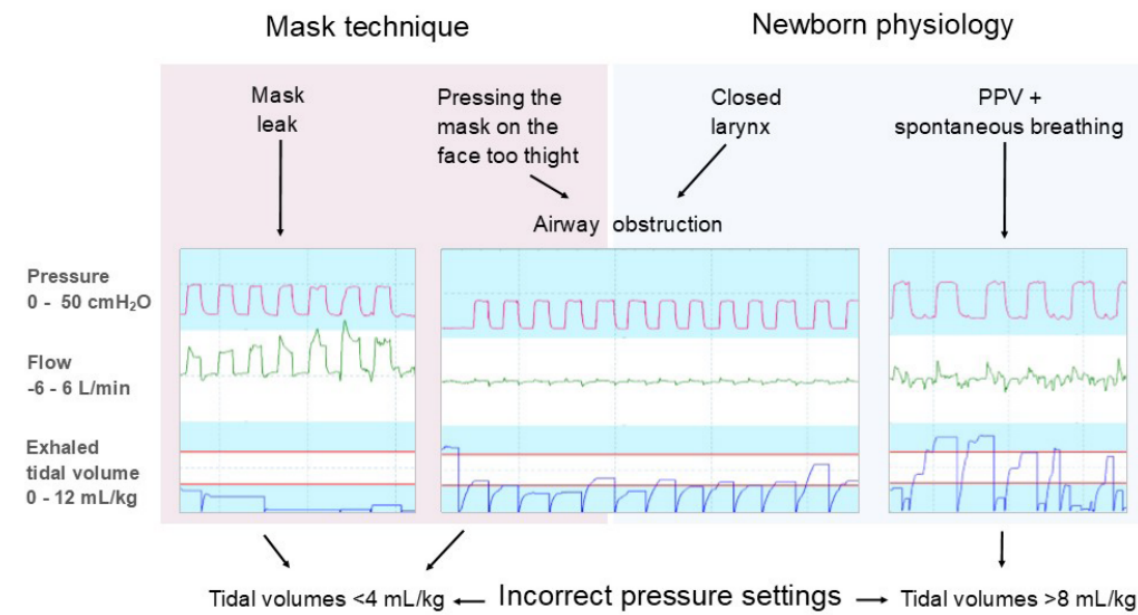


Figure 2.4: PPV as determined by pressure, mask technique and newborn physiology [47]

The red lines reflect The World Health Organisation's guidelines for safe and adequate tidal volumes for neonates (4-8 mL/kg) [14]. During mask leak, flow escapes and the infant only receives small tidal volumes. Physiological obstructions, such as the closure of the larynx under high pressure, also reduce flow. Alternatively, When the infant breathes spontaneously with PPV, tidal volumes can significantly deviate from safe ranges.

End tidal CO₂ (ETCO₂), the level of carbon dioxide that is released at the end of an exhaled breath, is also an important data point in assessing the effectiveness of resuscitation [48]. As CO₂ is only detectable at higher than atmospheric concentrations, if both physiological and cellular respiration has occurred, its presence in neonatal expiration indicates the infant is transitioning from placental oxygenation to pulmonary respiration. A lack of CO₂ indicates that the alveoli are still liquid filled and hence epithelial gas exchange cannot occur [49].

2.3 Respiratory Function Monitors

There is a consensus in the literature that graphically displaying respiratory parameters at the time of resuscitation improves the effectiveness of newborn ventilation [20][21][22]. Wood et al. stipulate that to improve mask leak, user technique must first be addressed [50]. Their manekin study at the Royal Women's Hospital Melbourne precipitated a median 24.1% reduction in leak from clinical staff after a demonstration from an experienced neonatologist, with a reduction of 8.8% occurring after simple written instruction alone. Building upon this study, Wood then investigated the use of a RFM for education [23]. Demonstrating correct technique in conjunction with a Florian respiratory monitor saw a reduction in mask leak from 24.3% to 13.1%. Furthermore, after then removing the monitor, the cohorts median leak rose to only 18.3%, demonstrating a RFM functioning as an educational tool. O'Curraun et al. further validated Woods results with a study across thirteen Australian hospitals [20]. An RFM provided real-time, objective leak, flow and volume during 1.5 hours of newborn ventilation training. The RFM was then taken away from the intervention group and both groups analysed under manekin simulation. The median face mask leak was 35% in the control group who never saw respiratory parameters, compared with 23% in the RFM visible group.

It is important to note that the International Liaison Committee on Resuscitation (ILCOR) still does not recommend a RFM in the practice of neonatal resuscitation and clinically their adoption has been limited to educational settings or the intensive care unit [43][51]. Furthermore, Schmolzer et al. found negligible improvements in performance from skilled senior staff, suggesting that an excessive graphical display may only be a distraction in this subgroup [21]. Additionally, whilst Schmolzer et al. demonstrated an improvement in ventilation from the use on an RFM overall, they highlighted that an inexperienced practitioner may misinterpret displayed waveforms. With this, it is again important to note that the large majority of the studies described above have been developed off of research conducted in high income environments with highly skilled clinicians. Whilst it is suggested that minimally educated practitioners would benefit even more from a RFM, this analysis is not available in the literature.

2.4 Technical Operation

Respiratory function monitors can be broken down into their three core subsystems of sensing, processing and outputting. Essential to respiratory monitoring is the measurement of gas flow over time, as it provides the basis for the calculation of tidal volumes, inspiratory/expiratory time, mask leak, respiratory rate and various other parameters [52]. RFMs transduce flow through sensors based on either hot-wire anemometry or differential pressure. Schena et al., state that a successful flow sensor must consider accuracy, sensitivity, linearity, frequency response, occupy a low inherent resistance, and a low dead space [53]. The data from these sensors is acquired and processed by a central processing unit in order to translate signal to respiratory parameter. This can then be outputted to the practitioner through some display. Many studies continually suggest that while the display of information from an RFM improves the effectiveness of newborn face mask ventilation training, work needs to be done to reduce the complexity of the displayed parameters [19] [54].

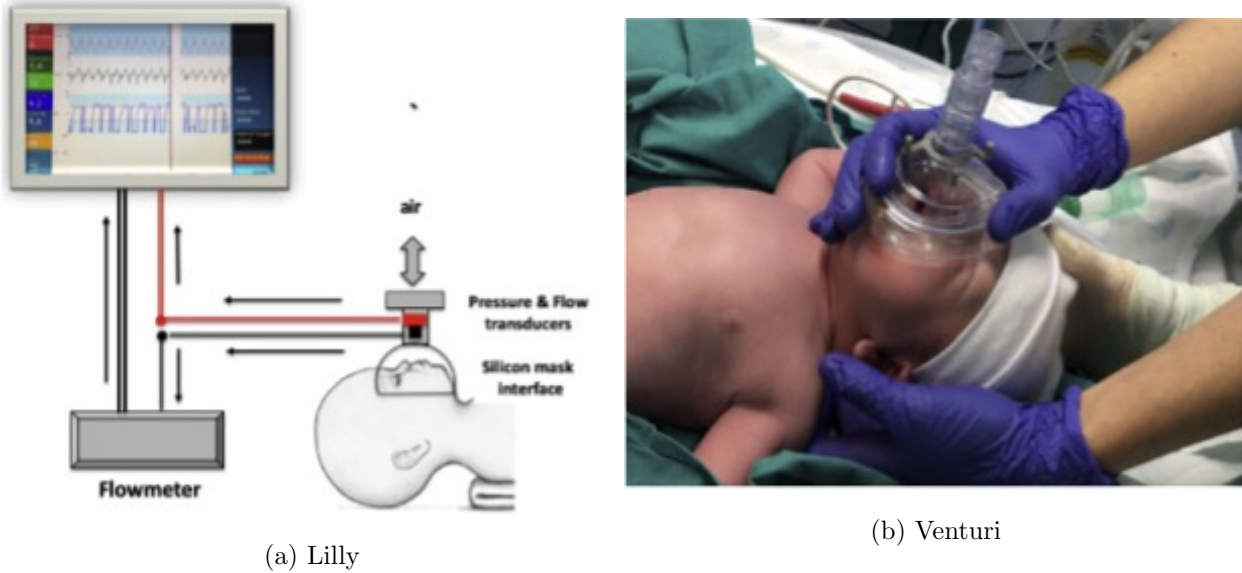


Figure 2.5: New Life Box (Advanced Life Diagnostics) RFM used in a clinical trial of Respiratory Rate Postnatal [19]

An important design consideration when constructing a flow sensor for an RFM or any pneumatic device, is Dead Space. Dead space is defined as any volume in the respiratory circuit that does not participate in gas exchange [55]. Pearsall et al. stress that the amount of apparatus dead space, measured by the volume of water required to fill the device, is of particular importance in paediatric ventilation [56]. Their modelling found that minimising internal volumes, relative to the weight of the infant, can avoid significant hypercapnia (buildup of carbon dioxide).

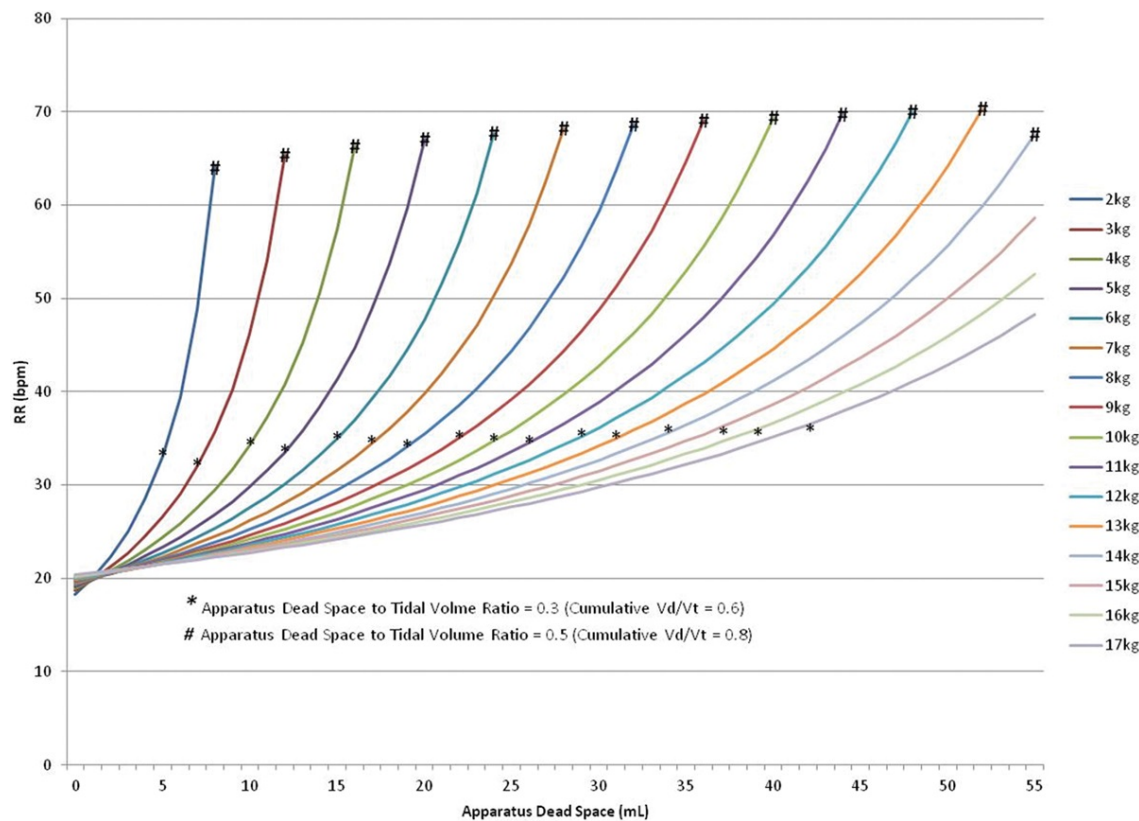


Figure 2.6: Respiratory rate (RR) to maintain normocapnia (40 mmHg) when varying apparatus dead space and patient weight. [56]

The above figure tracks the respiratory rate required to maintain normocapnia (40 mmHg) by variable apparatus dead space and patient weight. For a neonate of 2kg, we can see that any apparatus dead space may significantly alter pulmonary mechanics.

2.5 Hot Wire Anemometers

The predominant technology underpinning a RFM is the flow sensor. Hot Wire Anemometers (HWAs) are flow sensors based on convective heat exchange. Their operation was first defined by King in 1914, stating that heat removed from a hot-wire by a gas stream is linearly related to the square root of its velocity [57]. This system traditionally consists of one or more platinum wires, with flow either determined by a constant current model (flow determined by changes in wire temperature and resistivity) or more commonly a constant temperature model (flow determined by changes in the current needed to maintain the temperature). Both modalities employ the Joule effect, where the heat produced in a conductor is proportional to the product of its resistance and the square of its current:

$$h_w = \frac{1}{S_e(T_w - T_f)} I^2 R_f \quad (2.2)$$

Here, I is the current, R the resistance, S_e the surface area of heat exchange and T_w and T_f the temperatures of the wire and ambient gas [58]. When this transfer coefficient, h_w , is balanced by fluctuations in I , such fluctuations can be related to the velocity of the gas flow by:

$$h_w = A + B \cdot (\rho \cdot v)^n \quad (2.3)$$

Where, A and B are calibration constants at a specific geometry and gas composition, ρ the fluid density and v the velocity of gas flow. Traditionally n is set at $n = 1/2$, as defined by king, however, recent studies suggest that further calibration of this term may better account for measurement errors in low flow environments [59]. As a measurement of flow is dependent on the ambient environment and the composition of the gas, Talluru et al. propose a calibration method to account for multiple type sensor drift [60]. This method captures regular calibrations against a universal calibration curve that is accounted for in post-processing.

In addition to high sensitivity, HWAs offer fast response times and low impedance's to

flow and therefore ease of exhalation for the user. Such benefits see a sensor of this type being adopted in the Florian Respiration Monitor (Acutronic Medical Systems), a device extensively used in research today [61]. In spite of its strengths, HWAs are limited by their fragility, cost and inherent inability to distinguish the bi-directional flows of inspiration and expiration and thus determine accurate tidal volumes and mask leak [58].

However, some development has been done into HWAs that can discriminate flow direction, as first seen in 1975 by Yoshiya et Al. with a 3-wire technique [62]. This methodology places a central heated wire between two 'cold' wires, such that the wire downstream of the hot body is heated to a greater degree and polarity can be determined. Advancements saw this concept being applied in-silica as proposed by Putten et al. from 1983 to 2002 [63]. Putten eventually developed a bidirectional silicon flow sensor with an accuracy of 5.4% in regards to mass flow [64]. Whilst this technology has the potential to be a low cost and highly accurate alternative to traditional HWAs, they are not currently utilised in available RFMs [61]. Swiss company Sensiron, has recently had commercial success in developing a silicon-based flow sensor as seen in their 'CMOSens®' technology, however, price reductions have not been realised to a significant degree [65].

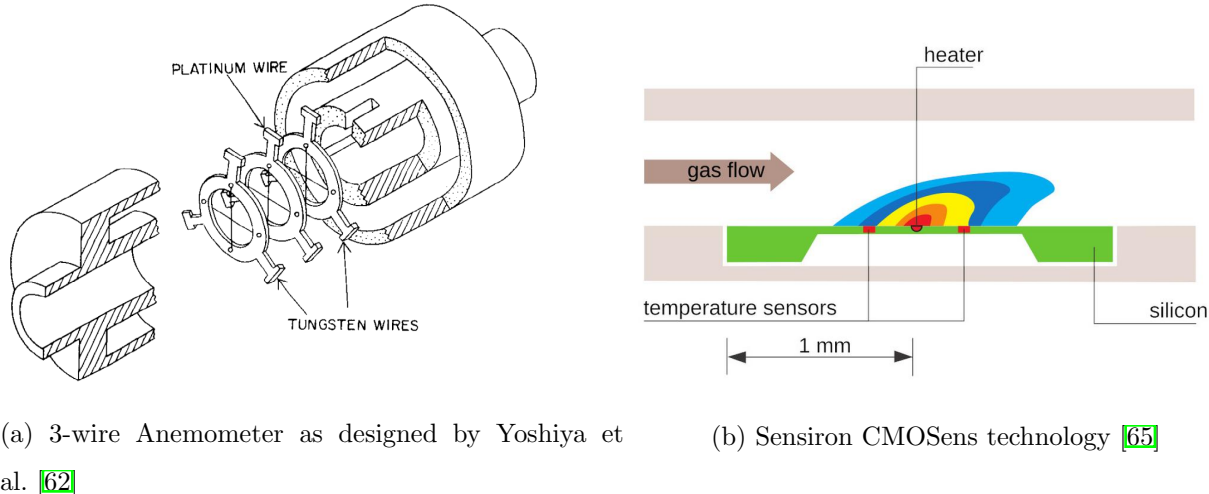


Figure 2.7: Development of sensing bi-directional flow in Hot Wire Anemometers from the 3-wire method to a hot body in silicon

2.6 Pneumotachometers

Pneumotachometers are flow sensors that relate the pressure drop of a fluid over a resistance (ΔP) to its volumetric rate of flow (Q). The design of a pneumotachometer varies based on the mechanism utilised to impart this resistance, being categorised as those that attempt to enforce a linear relationship between ΔP and Q and those that don't.

2.6.1 Non-Linear Pneumotachographs

Non-Linear systems include more traditional, unicapillary flow meters, in Venturi Tubes and Fixed Orifice Plates, where a change in pressure is imparted by an abrupt narrowing in the passage of gas flow. Their mode of operation is based on Bernoullis principle, described in the following equation:

$$Q = C \sqrt{\frac{2\Delta P}{\rho}} \frac{A_a}{\sqrt{(\frac{A_a}{A_b})^2 - 1}} \quad (2.4)$$

Where, C is a discharge coefficient to account for fluid viscosity, ρ the fluid density and A_a and A_b the upstream diameter of the pipe and the constriction diameter respectively. The simplicity and low cost of these devices make them very attractive, but the quadratic nature of their response incorporates a lack of accuracy in calibration. Additionally, changes in sensitivity usually have to come from changes to the overall geometry of the pipe, incorporating a difficult balancing act between sensitivity, pneumatic resistance and dead space.

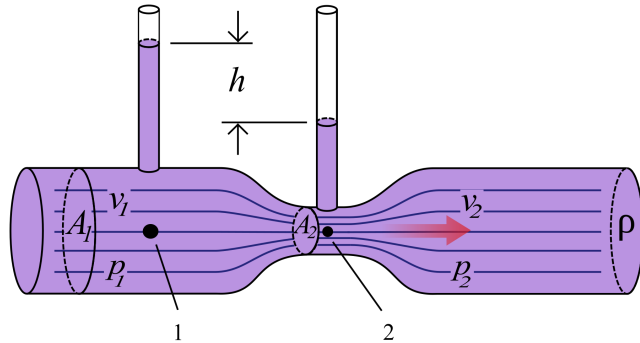


Figure 2.8: Venturi Type Pneumotacograph [66]

2.6.2 Linear Pneumotachographs

The Hagen–Poiseuille law assumes the relationship between ΔP and Q to be linear if laminar flow is consistently conserved (reynolds number ≤ 2000) [58]. For linear Pneumotachographs, mechanisms are introduced to enforce laminar characteristics such that this law consistently holds and the relationship between ΔP and Q can be described as follows:

$$\Delta p = \frac{8 \cdot \mu \cdot L}{\pi r^4} Q \quad (2.5)$$

Where L is the length of the funnel, r the radius, n the number of capillaries and μ the dynamic viscosity of the fluid. To try enforce a pseudo laminar regime, a Fleisch type pneumotachograph incorporates a bundle of capillaries, and a Lilly type, a fine mesh screen. They present the highest accuracy for pneumotachographs without introducing large impedance's to flow. The linear response curves can be easily fit, calibrated and scaled with a high degree of precision [67]. Additionally, These screens can easily be heated to prevent condensation and create stable fluid conditions. However, they are more fragile and expensive due to the demand on capillary manufacturing. The large effective surface area of the linearizing screens may also aid the formation of condensation that can deteriorate sensor sensitivity over time [68].

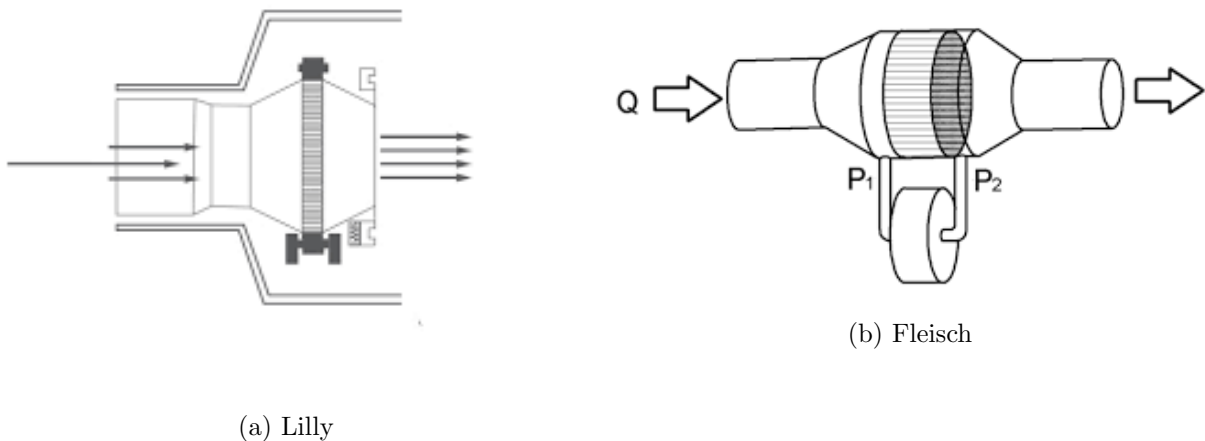


Figure 2.9: Comparision between Lilly and Fleisch type pneumotachographs [58]

Additionally, whilst this linear model is popularly accepted to describe the behaviour of these instruments, at very high or very low flows, this relationship is questioned [69] with many researchers now reaching for a second order polynomial called the Rohrer equation [70]. Thus, incorporating intricate mechanisms to enforce a linear response may be rendered redundant for the low flow environment of pediatric ventilation.

2.6.3 Constraints in Designing a Pneumotachometer

Irrespective of their design, we can see that the sensitivity of a pneumotachograph is always dependent on both the geometry of the system and the dynamics of the fluid. So, to increase sensitivity, the length can be increased or the radius restricted. However, in their review of the design characteristics of pneumotachographs, Giannella-Nieto et al present the balancing act between decreasing the internal geometry and increasing the pneumatic resistance and increasing the internal volume and introducing a harmful dead space [71]. Takatori responded to this in their development of a neonatal respiratory monitor, through the addition of two slits in the body of the sensor, to accountably increase the pressure difference over the resistance and thus increase sensitivity without incorporating potentially dangerous resistance to the neonatal breathing circuit [72].

Another major drawback in pneumotachographs is their reliance on the density and dynamic viscosity of the fluid (μ) and therefore their dependence on temperature, humidity and gas composition. In addressing this, many modern pneumotachographs introduce a heating element and thermistor for thermoregulation to reduce the collection of moisture at the sensor site [73]. Alternatively, Schena et al introduce further correction coefficients to account for the shift in sensitivity when gas conditions change [53], stating that, although frequent calibrations could reduce error, it is infeasible during mechanical ventilation.

Therefore, the delivery of adequate ventilation when introducing a pneumotacograph to a breathing circuit, is greatly influenced by minute changes to the parameters in equation (2.4). Therefore, informed design considerations must be taken into account for accurate measurements to be achieved.

2.7 Commercially Available Devices

Veerbek et al. investigated the accuracy in volume measurements of the most commonly available respiratory function monitors, tested by calibrated syringe with known volumes [61]. Results found that all were within a clinically acceptable range ($\leq 10\%$) but accuracy and dead space did fluctuate with each device. The Florian Neonatal RFM, incorporating a hot-wire anemometer, had an accuracy of $\pm 8\%$; the Philips Respironics Novametrix Monitor 3, with a fixed orifice differential pressure pneumotachometer had an accuracy of $\pm 3\%$; and the Advanced Life Diagnostics New Life Box, using a variable orifice pneumotachometer, had an accuracy of $\pm 5\%$. Both the Florian and the Novametrix had a dead space of 1ml, with the New Life Box operating on a dead space of 0.7ml.

Chapter 3

Commercial Considerations

The aims of this thesis were developed with insights from ResusRight. Their device, the Juno Training Monitor, addresses the aforementioned pitfalls of commercially available RFMs. The device has low power requirements and sits in line with the breathing circuit to provide continuous real-time feedback to practitioners. Indicators such as mask seal and tidal volume ensure clinicians are learning correct ventilatory technique.



Figure 3.1: Juno Training Monitor (ResusRight)

To derive displayed parameters, devices like this employ neonatal flow sensors, such as the SFM3400 mass flow meter, produced by Swiss company Sensirion. For the SFM3400, signal processing and digital calibration are on a single chip, assuring fast signal processing time, best-in-class accuracy and superior robustness [74].



Figure 3.2: SFM3400 Flow Sensor (Sensirion)

The sensor utilises a bidirectional hot-wire anemometer, where gas flow passes directly over sensor elements. Whilst this affords excellent sensitivity and accuracy (error of ± 0.05 standard liters per minute), electronics are not reusable between patients due to contamination. They have to either be disposed or re-purposed through an autoclave, negatively impacting cost and sustainability of the overall device. Therefore, the ability to design a low cost sensor, where electronics are separated from the flow chamber, would be extremely beneficial to the development of more accessible ventilatory technology globally.

Chapter 4

Methodology

It is suggested that in using differential pressure sensors, expensive electronics can be removed from biologics in the flowing gas to take every design precaution necessary to minimise contamination and the re-purposing of components [75].

It can be seen from section 2.6 of the literature review, that an effective RFM based on differential pressure measurements consists of four core subsystems: A source of resistance, a transducer to sense dynamics in pressure, a computational unit to convert gas flow to parameters of interest and a graphical display to engage results with the user. From the commercial considerations above, we can see that dramatic cost reductions would come from a sensor that does not have to be re-purposed between each patient. This thesis will therefore investigate the practicality of using differential pressure sensors to develop low-cost respiratory function monitors. For this proof of concept, the flow element, sensor and computational unit were designed to balance ease of ideation and cost. An analysis of the best graphical displays were not addressed in this experimentation and are left for future work, detailed in later discussions. The following sections will discuss constraints around selecting each component for the final flow sensor before explaining how each component was integrated, calibrated and characterized through testing. An overview of the subsystems contributing to the final flow sensing system is as below:

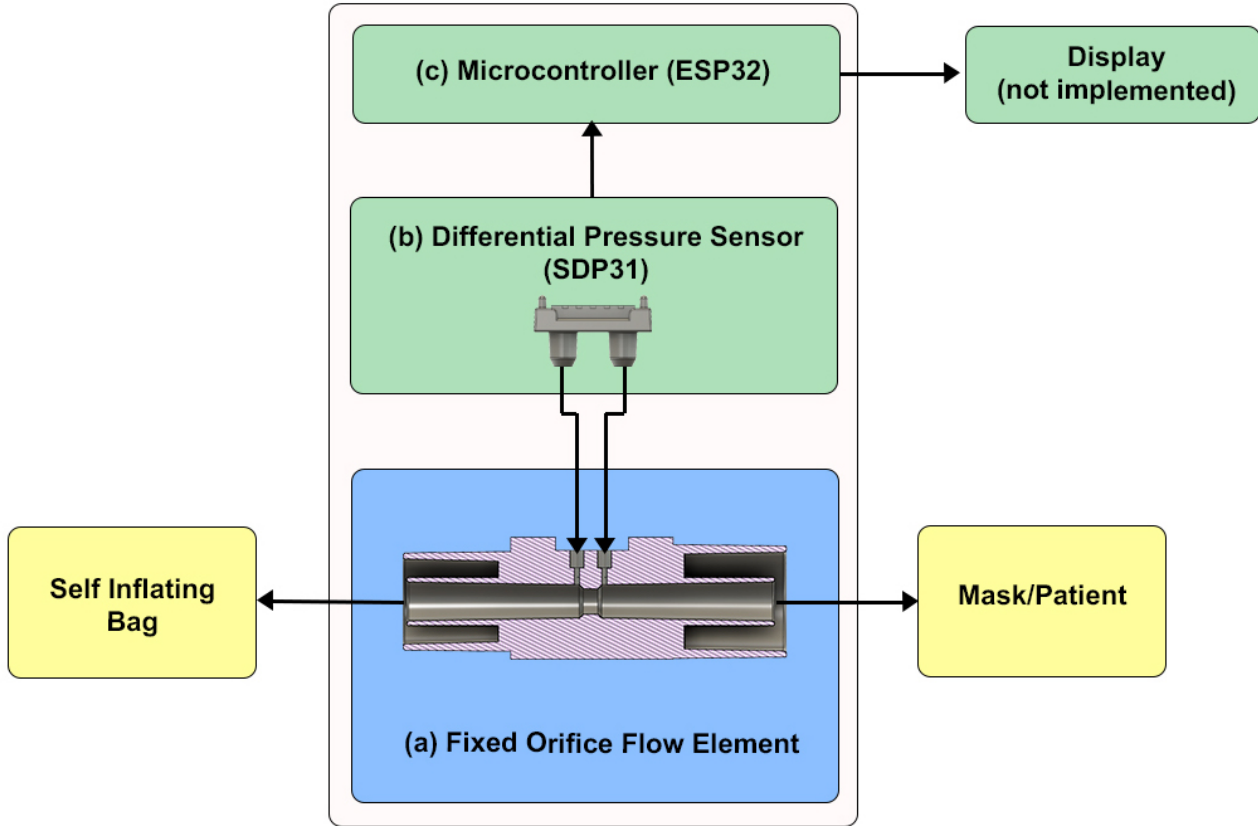


Figure 4.1: Flow Sensing System Overview

4.1 Selection of the Differential Pressure Sensor

Studies suggest that neonatal flow rates usually range between $\pm 6\text{-}8 \text{ L/min}$ through resuscitation [47][76]. However, to ascertain when things are going wrong and harmful volumes are being delivered, it is important to have a sensor that can operate over a wider range of flow. Therefore an aim for this thesis was set to define a system that can sense flow over ± 15 standard liters per minute (slm).

In selecting a differential pressure sensor, considerations around operating range, resolution, accuracy, cost and ease of implementation were assessed across commercially available sensors. It was decided that the SDP31 from Swiss manufacturers Sensirion would best fit the needs of this study. It has an operating range of $\pm 500\text{Pa}$, accuracy of $\pm 3\%$ pressure, the output is digital with a 16b resolution, connection to microelectronics is simple through an I2C bus and automatic temperature compensation is performed through an integrated chip. In addition to these characteristics, it is relatively cheap compared to other sensors on the market (\$27.01 in 300pc orders) and especially small (5x8x5 mm).

When a team at Fablab Brussels rapidly developed a low cost open source adult ventilator, they profiled a calibration curve between differential pressure and flow for their specific flow element [77].

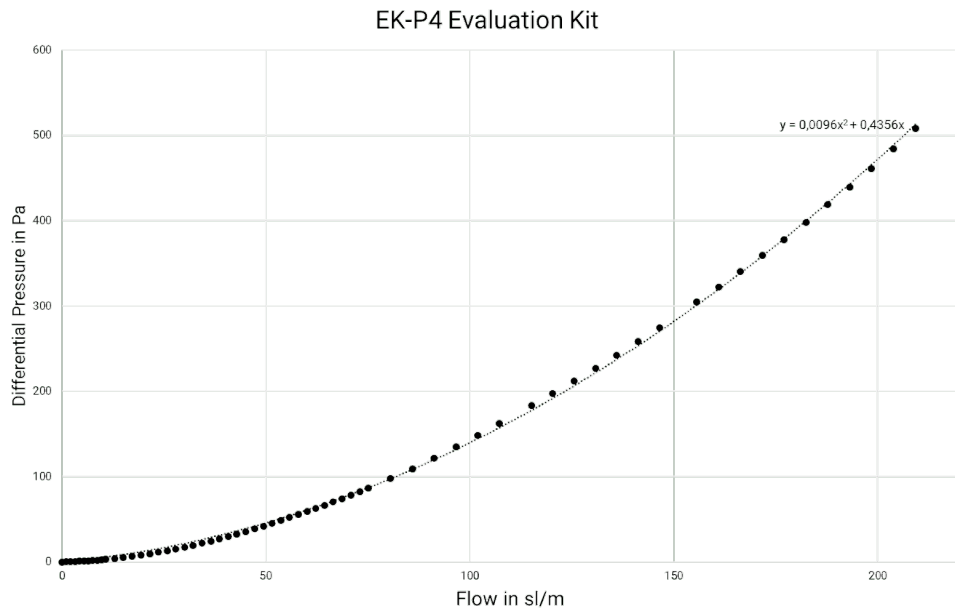


Figure 4.2: Calibration Curve BREATHNEY Sensor Module [77]

We can see that at 20 slm the sensed differential pressure of their system was only 13Pa. Whilst this could inform the choice towards the SDP32 sensor with an operating range of ± 125 Pa and a slightly lower zero point accuracy (0.08 Pa compared to 1.0 Pa in the SDP31), it is important to note that the Fablabs system was built for adult ventilation and was not focused on the physiology of the neonate. In their development of a capillary like pneumotachograph for neonatal ventilation, Schena et al. produce a calibration curve that reaches its maximum at just below 500Pa at 10 L/min.

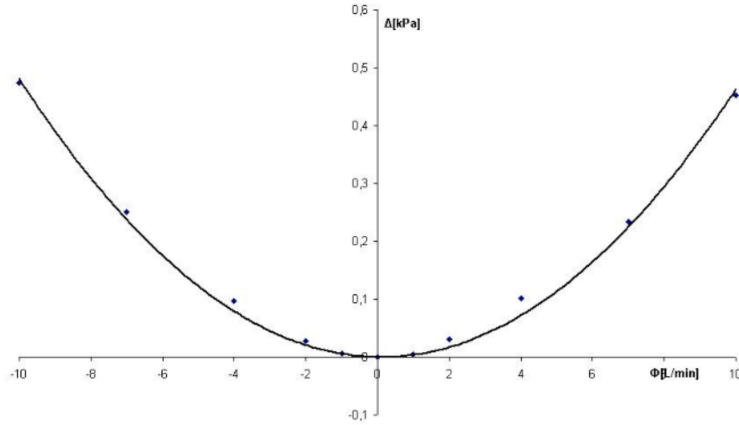


Figure 4.3: Calibration Curve For Neonatal Flow Sensor Assessed by Schena et al. [70]

In this context, larger pressure drops are needed to be generated to improve the response of the sensor at low flows. As the SDP32 has the same resolution and full span accuracy as the SDP31, it was decided to go with the larger operating range for prototyping and ideation.

4.2 Computational Unit

To communicate with the SDP31, the sensor was connected via the I2C protocol to an ESP32, a common microcontroller selected for its inexpensiveness and low power consumption. As the sensor is board mountable, a commercialised device could include a custom PCB and battery source but the microcontroller was used in this case for fast prototyping and ideation. Code was written in C++ with Object Orientated Programming in mind, to drive reading

and the normalisation of sensed values. Classes were written to initialise the device, soft reset the sensor and start continuous temperature compensated differential pressure sensing. Samples were then read at a rate of 300Hz to match this device to existing protocols in ResusRight’s Juno Training Monitor for later experimentation.

4.3 Design of the Flow Element

4.3.1 Constraints

The goal of designing a pneumotachograph or ‘Flow Element’ is to increase the sensitivity of gas flow measurements while not introducing pneumatic resistance or unused dead space to the breathing circuit [58]. These design considerations are quantified for ventilators in ISO 10651-4, where constraints that impact resistance (R), dynamic compliance (C_{dyn}), and resistive work of breathing (WOB) are presented for individuals $\leq 10\text{kg}$. Minimum test conditions for these values can be found in Appendix A.1. Most importantly, the pressure generated at the patient connection port, that is, where the mask meets the infant, shall not exceed 0.5 kPa at 5 L/min flow. Additionally, the standard states that apparatus deadspace shall not exceed 5 ml + 10 % of the minimal delivered volume (20ml in patient body masses $\leq 5\text{kg}$). However, this dead space is for the entire apparatus, not specifically for the flow element, and thus, dead space must be significantly minimised beyond this 5ml limit.

4.3.2 Early Prototypes

An early prototype was developed to test fabrication processes and start ideation around design geometry. Most studies in the literature implement a Fleisch like design for the pneumotachograph where bundled capillaries enforce a laminar regime, maintaining a linear relationship between differential pressure and flow [67][78]. However, these studies address adult ventilation. Under the specific conditions of neonatal ventilation, the benefits of using a linearizing screen may not be realised. Specifically, from section 2.6.2 of the literature we can assess that in the low flow environment of observed neonatal respiratory patterns, designs to enforce laminar flow are rendered redundant, especially considering that at low flows the

relationship is rarely linear irrespective of the gas condition [58]. Additionally, multiple flow channels like in a Fleisch design increase the effective surface area of the sensor, lending to a build up of humidity that can impact upon the consistency of calibrated measurements, add complexity and manufacturing costs, and even block the passage of regurgitation [68]. Therefore, to reduce complexity, internal surface area and dead space, a Venturi like design was first implemented, reflecting studies like that of Jacq et al. [66].



Figure 4.4: Venturi Like Design for Early Prototype

From the initial design we can see that the sensor was removed from the main gas flow through port holes that sit 2.6mm away, to try and remove electronics from flowing biologics. To easily interface with any neonatal breathing circuit, the prototype incorporated standard pneumatic connectors as defined in ISO 5356-1. For neonatal equipment, 15mm cone and sockets were integrated, with geometry constraints in line with this standard (presented in appendix A.2).

From the study by Pearsall et al. into the impact of apparatus deadspace on the paediatric patient, we can see that, for low-weight infants, any appreciable dead space added to a circuit greatly influences normocapnia [56]. Apparatus dead space was minimised in this design by minimising internal volumes. The flow element incorporated an internal tube in the body of the device, with the first prototype measuring a dead space of <1ml, competitive with commercial RFMs developed for research [61].

From equation 2.4 of the literature review we can see that the sensitivity of a Venturi pneumotachograph is dependent on the geometry of the flow element, such that, increasing the ratio between the upstream diameter of the pipe and the constriction diameter would see a marked increase in sensitivity. Jacq et al use a constriction diameter of 1.8mm in their

venturi tube for low flow measurements. However, with the smallest neonatal endotracheal tube measuring only 2.5mm, there was a concern that utilising such small diameters would introduce harmful pneumatic resistance to the pulmonary mechanics of the infant. Additionally, their device was for ultra-low measurements where the maximum sensed flow was only 4 L/min. For this initial prototype, an estimate of 3 mm for the constriction was used.

4.4 Manufacturing and Assembly

To build each prototype, flow elements were 3D printed to allow the fast verification and validation of design iterations. Stereolithography (SLA) was used, where light-reactive thermoset resins are pulled from a reservoir and allowed to set layer by layer. The resin of choice was Formlabs 'Tough 2000', chosen for it's rigidity and reproducibility between prints. As the operation of a pneumotachograph is defined by its geometry, testing required a relatively high level of precision to scale and morphology. Prints were always set on an angle to allow the run-off of excess resin. After printing, they were washed for 20 minutes in isopropyl alcohol (IPA), allowed to dry and then cured in an ultraviolet light chamber for 60 minutes at 70°C in line with the manufacturers guidelines.



Figure 4.5: 3D-printed Flow Elements After Curing for 60 minutes at 70°C

4.5 Preliminary Validation

Once the first prototype was printed it was tested with common neonatal apparatus to test pneumatic connectors. The flow element was pushed into an Ambu infant resuscitator until no further movement could be made. It was found that the connection was tight and when occluding all exit holes and using the resuscitator, no gas was observed escaping from the connection point. Whilst this is a very informal test, it acted as a preliminary verification that the cones and sockets were designed correctly. More formal procedures such as Pressure Decay Tests are discussed in later sections.

The device was then assembled with sensor components, connected to both a SIB and a 300ml IMT infant test lung, to assess the systems differential pressure response to bidirectional flow. Manual pulses were produced by hand on the SIB to simulate a resuscitative environment. We can see from the below graph that the forward response has a high degree of noise and registers no significant response to flow.

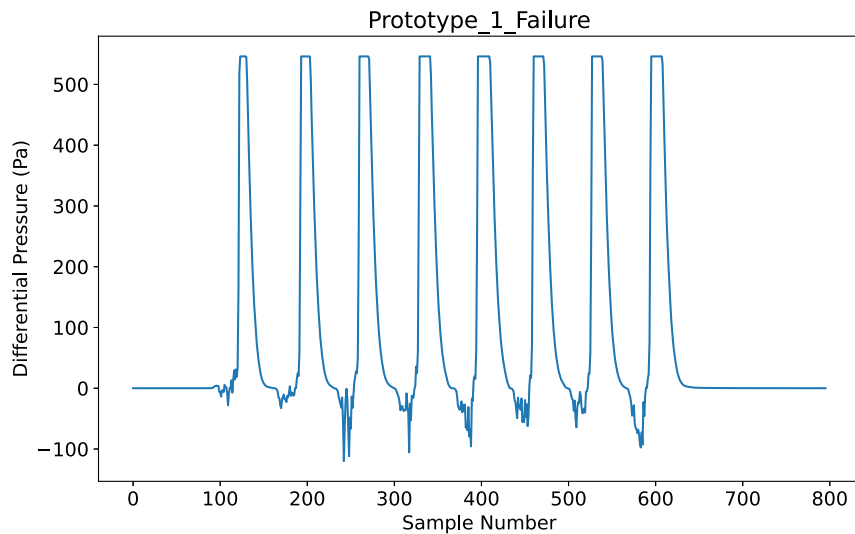


Figure 4.6: Simulated Infant Breath Signal Prototype 1

It was thought that this could be due to blockages due to fabrication, however, upon checking each through-hole under magnification, no visible defects were spotted. Additionally, a second device was tested and expressed the same response. This suggested that the Venturi design was not operating bidirectionally. Moreover, we can see that on the successfully registered expiration's, the sensor is hitting the maximum differential pressure for the SDP31 (544 Pa). Therefore, further attention had to be made to both the bidirectionality and operating range of the system.

4.6 Improvements

To better enforce bidirectionality, the next iteration involved a simple fixed orifice pneumotachometer. This design involved a constriction plate where both inspiratory and expiratory paths behave symmetrically. The sensor sits 2.6mm away from flowing gas, separated by 0.8mm through-holes. Two supports were added to the top face of the element to take stress away from the SDP31 sensor tubing in line with the companies application note. The following figures display the CAD design of the fixed orifice pneumotachograph followed by a final integration of the system

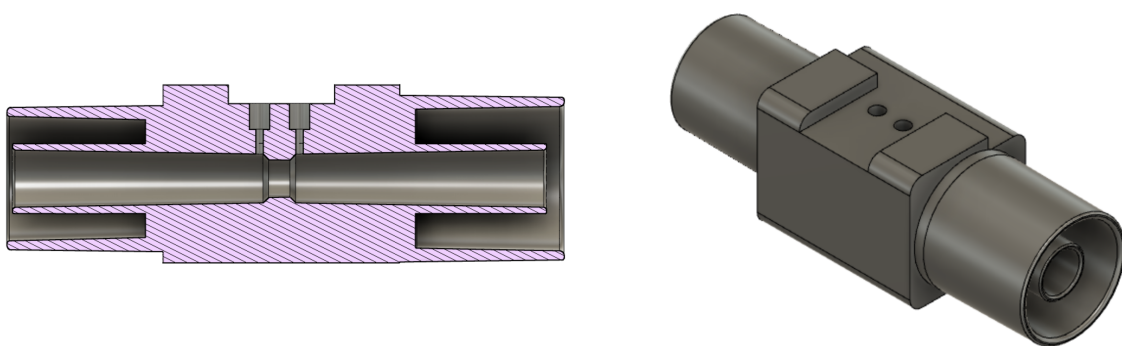


Figure 4.7: Fixed Orifice Pneumotachograph (3.5mm)

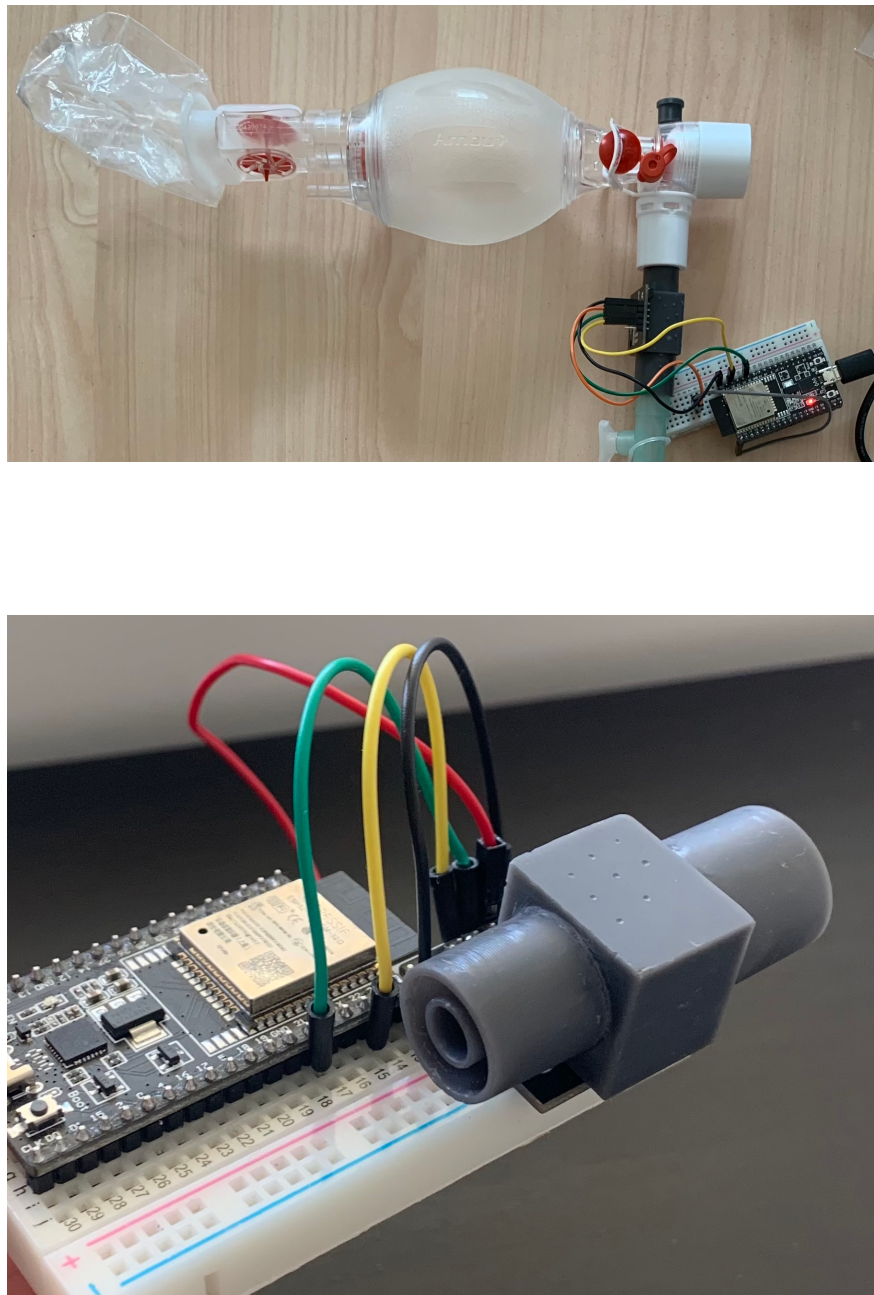


Figure 4.8: Full Integration of the Flow Sensor Attached to a Self Inflating Bag and Standalone

In finding the ideal operating range for the sensor, an analytical approach was first taken. The relation of differential pressure to flow for a fixed orifice pneumotacograph is as below:

$$Q = C \sqrt{\frac{2\Delta P}{\rho}} \frac{A_a}{\sqrt{\left(\frac{A_a}{A_b}\right)^2 - 1}} \quad (4.1)$$

If the differential pressure is set at the maximum value of our sensor (544 Pa) and the upstream diameter as the diameter of the entrance (5.22mm), the constriction diameter can be varied to find the theoretical maximum sensed flow for each design. The discharge coefficient and density were set to a standard of 0.788 and 1.2431 kg/m³ respectively, in line with suggestions by Hollingshead et al. [79].

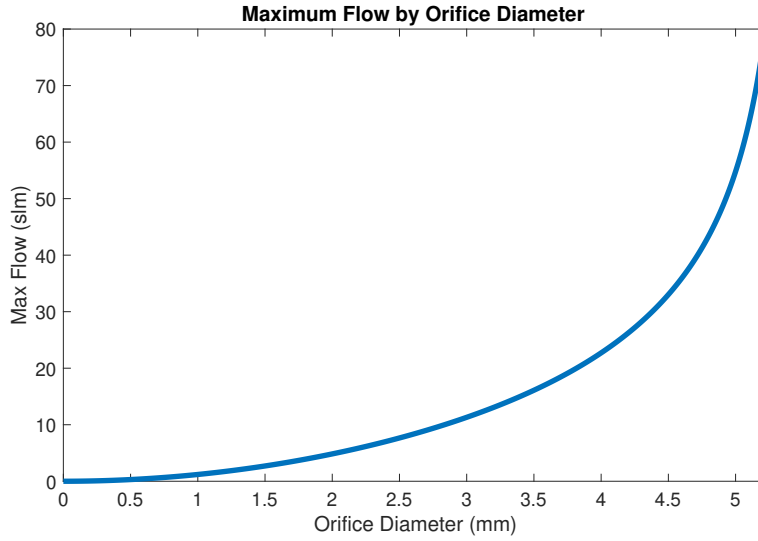


Figure 4.9: Analytical Estimate of Maximum Flow by Orifice Diameter

From the above curve it can be seen that with a 2.5 mm orifice, the theoretical maximum flow the system will be able to sense will be 7.6 slm and with a 4 mm constriction, 22.76 slm. However, the analytical case is ideal and lossless, not compensating for turbulence [75]. Further tests were required to ascertain the true behaviour between differential pressure and flow in this projects pneumotachograph, comparing how such an analytical classification of these systems would relate to experimental observation.

4.7 Testing

Four fixed Orifice Pneumotachographs were selected for this study. All flow elements were 59.4 mm in length with standard pneumatic connectors as described in section 4.3.2 above. The tubes internal diameters were 5.227 mm at the start of the orifice plate. The only variable changed between prints was the size of the orifice, with constrictions of 2.5, 3, 3.5 and 4 mm tested.

The experimental assessment of each pneumotachograph was carried out with a threefold aim: (i) to obtain their individual calibration curve to assess operating range and sensitivity (ii) to evaluate the difference between experimental observation and numeric prediction (iii) to investigate any potential interference the pneumotachograph may have on respiratory mechanics through an analysis of static pressure and dead space.

Each flow element was printed inline with the manufacturing methodology outlined in section 4.4 above. After each print the through holes were tapped with a 0.8mm pin drill to clear any obstructed resin and inspected under magnification for any deformities. Once passed, searching for major deformities such as blocked passages, each sample underwent the below testing.

4.7.1 Calibration of the Flow Sensors

The calibration curve relates the pneumotacographs differential pressure response to a range of flows. Tests aimed to validate effectiveness through an assessment of each sensors operational range, sensitivity and bidirectional capabilities. In an ideal world, this assessment would be performed on traceable flow analyses. This was planned to be an IMT Analytics FlowAnalyser PF302. However, due to the nature of the COVID-19 pandemic, experimentation was limited to rudimentary bench-top tests with what was available at hand.

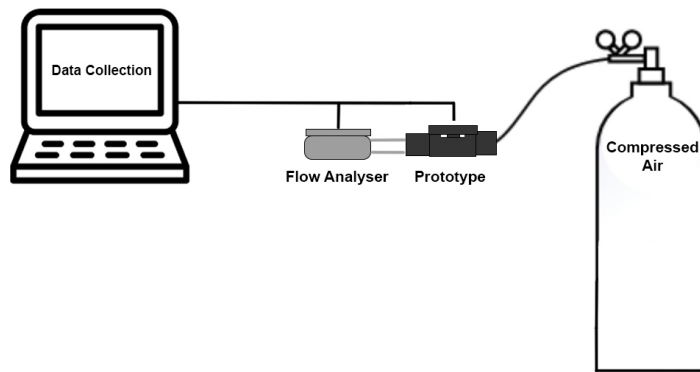


Figure 4.10: Experimental Setup: Differential Pressure vs Flow

For this test, a compressed air canister was placed in-line with the prototype through a long segment of medical tubing measuring approximately 1.5m. The tubing upstream of the prototype was maintained straight, to minimise the effect of turbulence through calibration. The prototype was then connected by a straight pneumatic connector to a Juno Training Monitor provided by ResusRight, herein labelled the 'control'. This device has a known accuracy (0.05 slm) and operated as the flow analyser. The outlet port of the flow analyser was open directly to atmospheric pressure.

Each test began by starting the prototype and the control device simultaneously to align measurements. The canister was then opened carefully until some measured flow was registered on the control. If the flow jumped above 2 slm this process was restarted. Once a flow (≤ 2 slm) was registered, it was held for 3 seconds before being manually increased by approximately 1 slm. This was repeated, in a stepped manner, until the sensor maxed out or the flow on the control reached a value of 30 slm. This process was repeated 3 times.

Once this was completed for the forward direction, the prototype was reversed and the methodology replicated to investigate the bidirectional nature of each design. These steps were completed for each constriction size.

Each measured step in flow was then averaged as a data point for subsequent analysis. Data cleaning had to be performed to remove unwanted artefacts in the signal. Any removed

value was replaced with an average of the entry directly before and after it. An example of the raw experimental signal for the 3.5mm constriction can be seen in appendix A.3.

4.7.2 Assessment of Flow Rate Error

After characterising the relationship between differential pressure and volumetric flow, each prototype was individually calibrated with a second order polynomial as suggested by Schena et al. [70]. To test the accuracy of this calibration, values at low, medium and high flows were assessed against the control. The experimental setup was the same as outlined in section 4.7.1 above. However, instead of successive steps of 1 slm, flows were held for 10 seconds at approximately 5, 10 and 15 slm, corresponding to a low, medium or high flow. These values had to be estimated from the regulator and were therefore not precise. The aim of this experiment was to ascertain the error between the control and the now calibrated flow sensor.

4.7.3 Performance Validation

An assessment of each flow element under simulation was performed. The prototype was placed inline with a infant SIB, a Juno Training Monitor and a 300ml IMT infant test lung to simulate a resuscitation (An image of this setup can be found in Appendix A.4.)

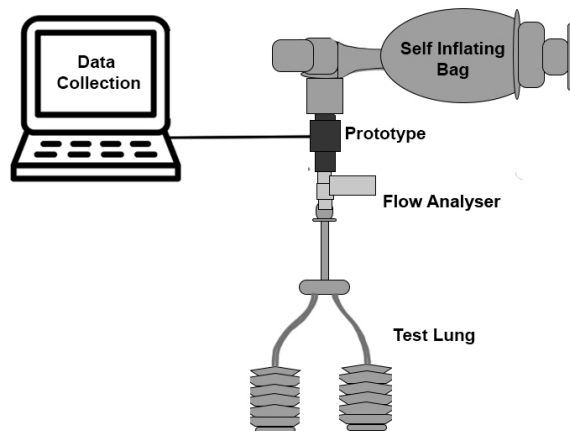


Figure 4.11: Experimental Setup for Performance Validation Testing

The self inflating bag was pumped at a variety of frequencies. Waveforms denoting flow rate under simulation were captured to visually assess temporal dynamics of the system compared to the control.

4.7.4 Computational Fluid Dynamics: Testing Resistance

As discussed in section 4.3.1, a risk of making highly sensitive pneumotachographs, is the introduction of resistance to respiratory mechanics. Specifically, ISO 10651-4 states that the pressure generated at the patient connection port should not exceed 0.5 kPa at 5 L/min flow. This limit was tested through computational fluid dynamics. The CAD model for each design was entered into Autodesk CFD. A simulated 5 L/min was added to the proximal opening that would be closest to the patient. A constant temperature of 25°C was set. The flow element material was best matched as moulded ABS and the fluid was dry semi-turbulent air. The simulation was run for 100 steps tracking both velocity and static pressure.

Chapter 5

Results

5.1 Calibration Curves

The operating range and sensitivity was assessed via calibration curve, where the experimental setup outlined in section 4.7.1 profiled the relationship between volumetric flow and differential pressure.

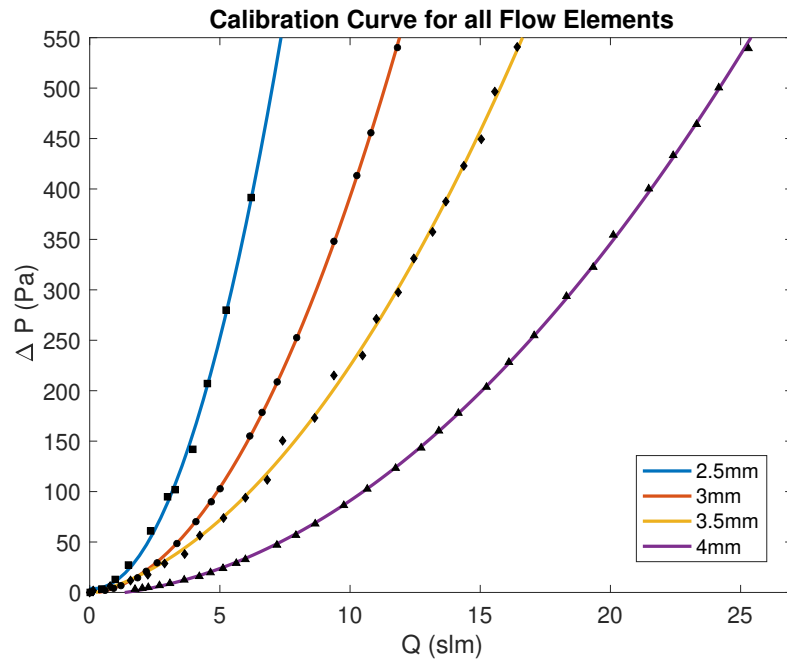


Figure 5.1: Calibration Curve for 2.5, 3, 3.5 and 4mm Fixed Orifice Pneumotachographs

Size (mm)	Max Flow (slm)	Sensitivity 0-5 slm (Pa/slm)	Sensitivity 5-10 slm (Pa/slm)	Sensitivity 10-15 slm (Pa/slm)
2.5	7.43	64.92	-	-
3.0	11.85	64.61	81.80	-
3.5	16.82	14.29	31.75	48.63
4.0	24.24	6.01	14.52	24.10

Table 5.1: Calibration Results: Maximum Sensed Flow and Sensitivity by Orifice Size

It can be seen that larger diameter constrictions offer larger operating ranges but a reduction in sensitivity. Only the 3.5 and 4 mm designs passed the aim of a ± 15 slm operating range with maximum sensed flows of 16.82 and 24.24 slm respectively. Sensitivity was assessed by region, where sensitivity was related to the derivative of a piece-wise linear function, fit between 0-5, 5-10 and 10-15 slm on the calibration curve. The 4 mm orifice precipitated a poor result at low flows, with a gradient of only 6.01 Pa/slm compared to 64.61 and 14.29 Pa/slm for the 3 and 3.5 mm orifice's respectively. The piecewise function for the 3.5 mm orifice is as below:

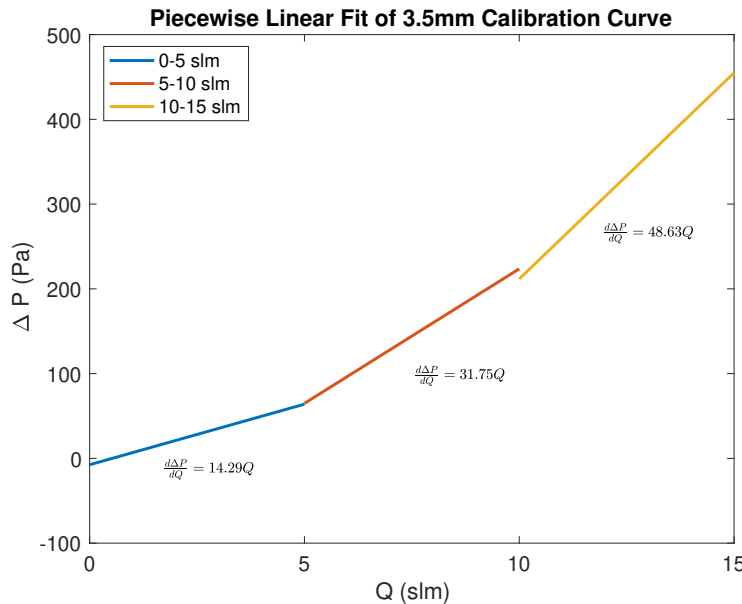


Figure 5.2: Sensitivity assessed by Low, Medium and High Flow Ranges

With only 4 samples tested, there was a statistically insignificant amount of data points to describe the relationship between orifice size and maximum sensed flow [80]. However, a possible quadratic trend is presented below:

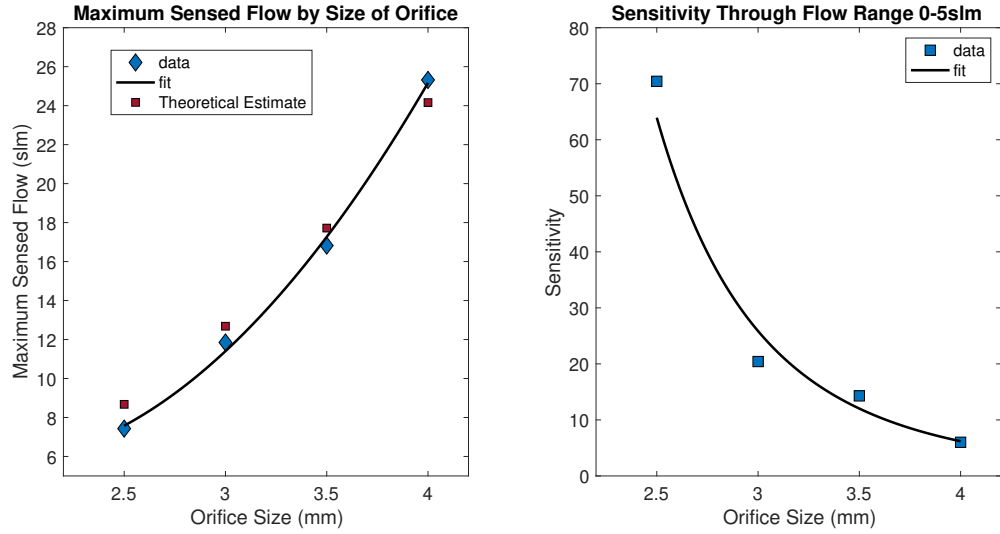


Figure 5.3: How Maximum Sensed Flow and Sensitivity Varied with Orifice Size

Included in the figure, is the predicted maximum sensed flow from the theoretical estimate from equation 2.4 of the literature review. We can see that the difference between the predicted and measured maximum flow is relatively consistent between designs with an average difference of only 1.035 slm with a standard deviation of only 0.2slm.

Size (mm)	Predicted Max (slm)	Measured Max (slm)	Difference (slm)	Error (%)
2.5	8.67	7.43	1.24	14.34
3.0	12.68	11.85	0.83	6.56
3.5	17.72	16.82	0.9	5.34
4.0	24.15	25.32	1.17	4.81

Table 5.2: Difference between Observed and Predicted Maximum Sensed Flow

5.2 Experimental Outcome vs Analytic Prediction

This comparison between the theoretical estimate and the experimentally derived values was further assessed by comparing the full calibration curve. Firstly, the correlation between flow and differential pressure was not linear, but described well by quadratic terms, evident in a high R^2 value for each fit ($R^2 = 0.99$). Figure 5.4 shows each calibration curve, the estimated fit by second order polynomial and the theoretical fit, produced from equation 2.4.

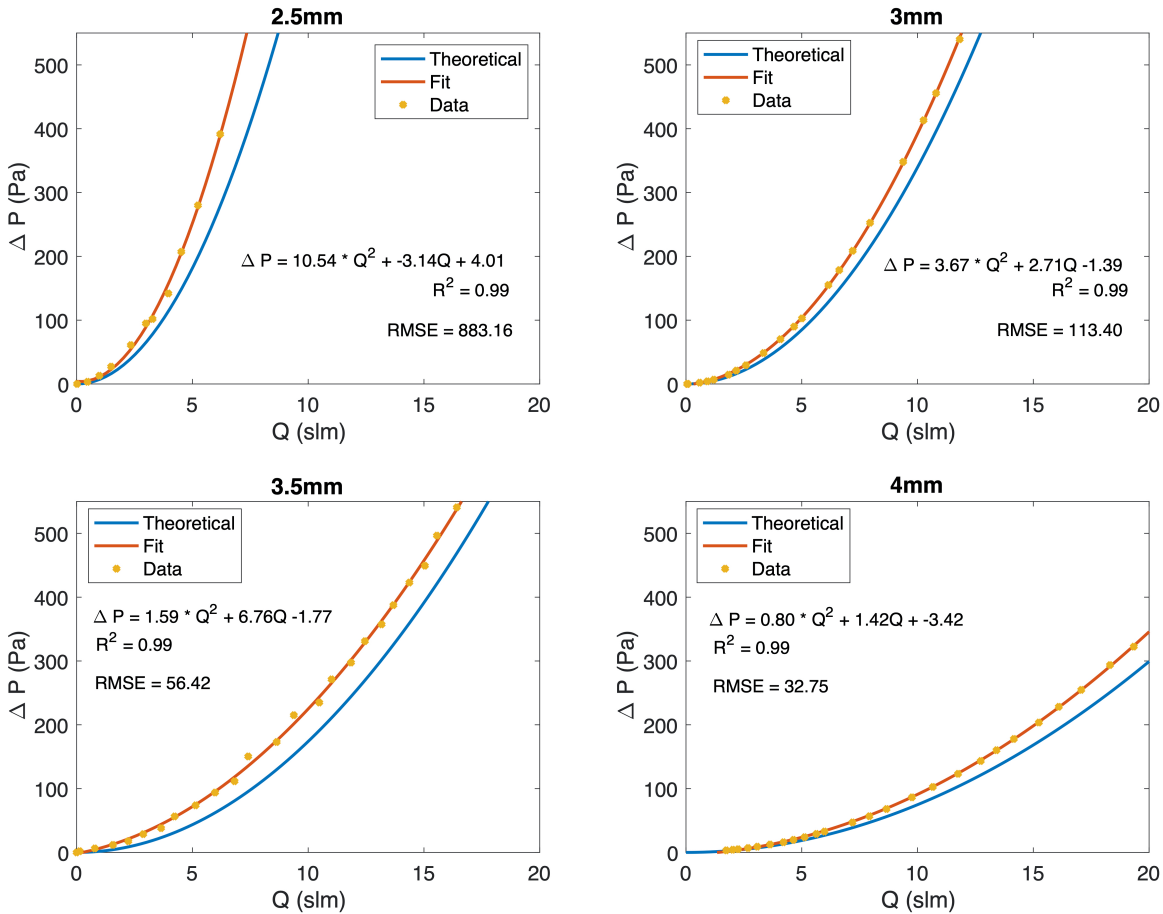


Figure 5.4: Calibration Curves Plotted with Their Theoretical Estimate

Data points were considered as the mean of each step. As the flow at each data point changed significantly with each sample, due to highly inconsistent tooling (screw valve on the gas canisters regulator), a sophisticated measurement of uncertainty could not be produced.

The difference between the experimentally derived curve and the theoretically predicted curve was assessed via the value of the Root Mean Squared Error (RMSE):

$$RMSE = \sqrt{\sum_{i=1}^M \frac{(\Delta P_1 i - \Delta P_2 i)^2}{n}} \quad (5.1)$$

where $\Delta P_1 i$ is the pressure drop at the i th flowrate on the fitted curve and $\Delta P_2 i$ is the pressure drop at the i th flowrate expressed by the theoretic estimate. n is the number of flow rates used to fit the two curves, in this case, 100. A summary of the RMSE by orifice size is as below:

Size (mm)	RMSE (Pa)
2.5	883.16
3.0	113.4
3.5	56.42
4.0	32.75

Table 5.3: Summary of RMSE Between Predicted and Experimentally Fit Curves

Whilst the theoretical estimate from section 5.2 above was relatively strong at predicting the maximum sensed flow, the entire calibration curve was not well predicted. However, the error decreases as the orifice size increases and the calibration curve flattens. Whilst this may not effect the performance of individual devices it highlights that the prediction of their behaviour analytically, from the basic equation for unicapillary pneumotachographs, is not well described.

5.3 Assessment of Bidirectional Behaviour

In preliminary validation, reviewed in section 4.5 above, an area of concern was the asymmetrical nature of the flow sensor. This was assessed in the final fixed orifice design by comparing inspiratory and expiratory data. For this test, the forward and reverse direction underwent the same experimental test setup, quadratics fit to the data points and the similarity between these fits analysed again through the Root Mean Squared Error. This analysis showed that the inspiratory and expiratory response of each flow element was relatively consistent. The 2.5 mm expressed the worst alignment, with a RMSE of 254.12 Pa compared to a RMSE of 29.49, 5.94 and 5.32 for the 3 mm, 3.5mm and 4 mm orifice's respectively.

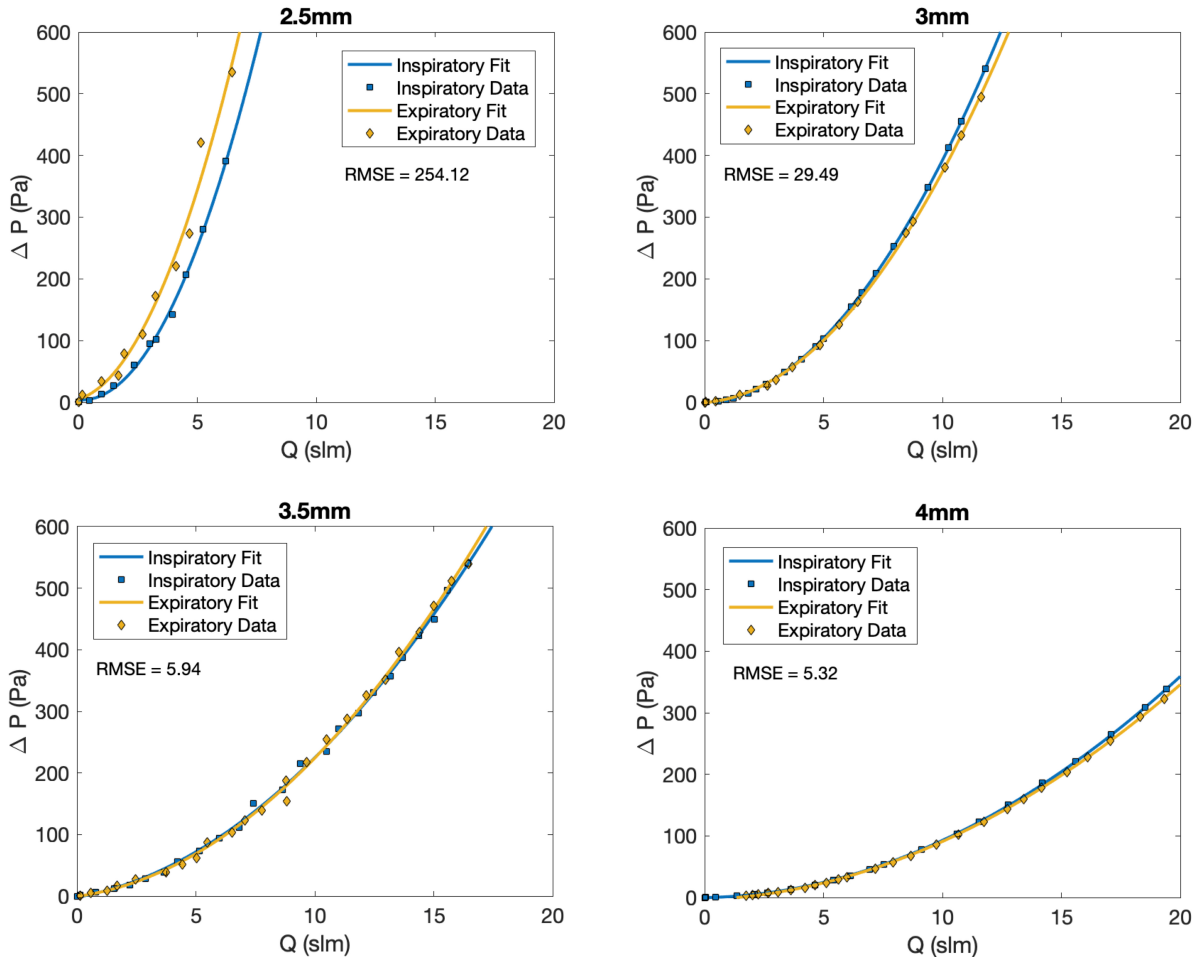


Figure 5.5: Analysis of Symmetry Between Inspiratory and Expiratory Flow for Each Orifice Size

5.4 Assessment of Flow Rate Error

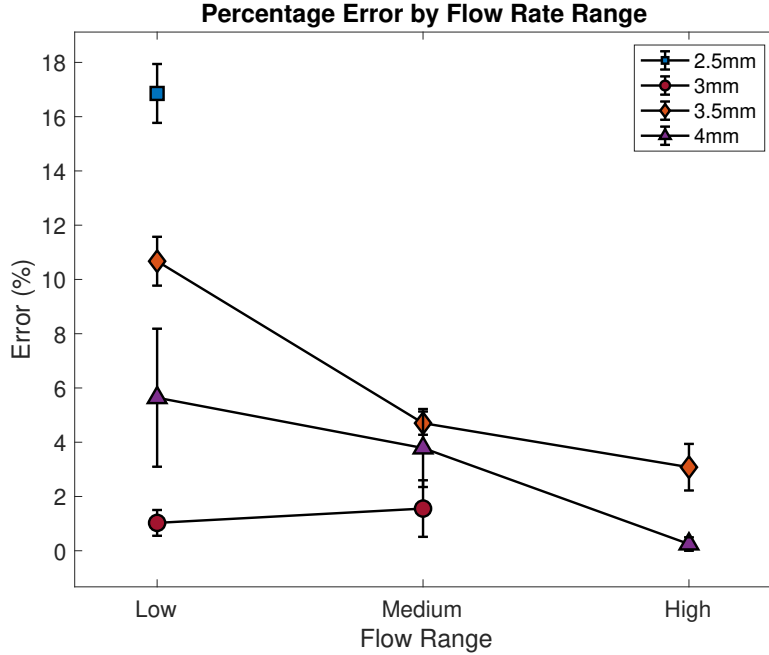


Figure 5.6: Flow Error of Prototypes Against the Control. Ranges are Split into Low (0-5 slm) Medium (5-10 slm) and High (10-15 slm) Flow

All results are reported as mean \pm uncertainty, calculated considering a student t-distribution with a 95% confidence interval (in line with [68]). It can be seen that for the 2.5mm and 3mm orifice sizes that a flow recording was only viable for the low and low and medium ranges. This corresponds to their individual operating ranges assessed in section 5.1 above. The 2.5mm measured the highest error at 16.86% compared to the control. The 3mm registered a very low error across both low and medium flow ranges at 1.03 and 1.55% respectively. Both the 3.5 and 4mm followed similar trends, with large error measured at low flows that fell as the flow rate increased. What was unexpected was the lower error reported by the 4mm orifice plate at all ranges compared to the 3.5 mm. The uncertainty in measurements for the 4mm was found to be very large at low flows (2.544%).

5.5 Performance Validation

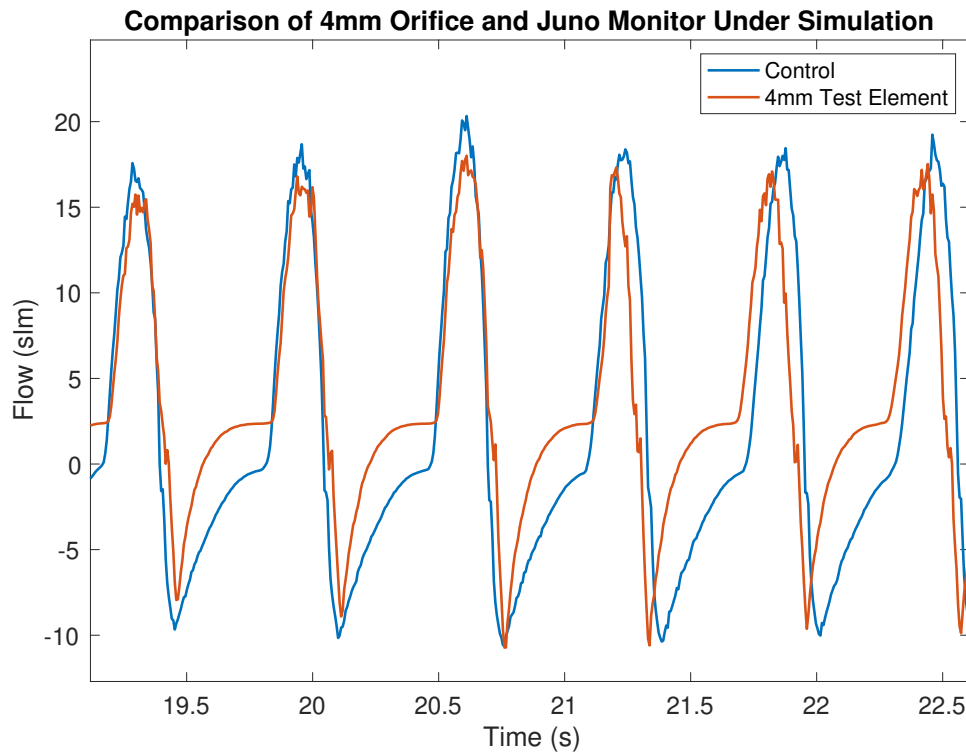


Figure 5.7: Wave-forms of 4mm Orifice Under Test Lung Simulation

The above figure depicts the test lung simulation of the 4mm orifice against the control. Whilst they are closely matched at the peaks of the breaths, error is introduced to the waveform at low flows. At the higher flow rates, noise can be seen on both the control and the test element. This noise was further seen across all test elements, documented at the peak of their wave-forms in figure 5.8 below. As the flow increases, the signal introduces uncertainty and noise. This can be seen on all wave-forms but especially on the negative of the 3.5mm orifice. Moreover, this simulation confirmed that the 2.5mm design has an operating range that is too low, maxing out the sensor on each pulse.

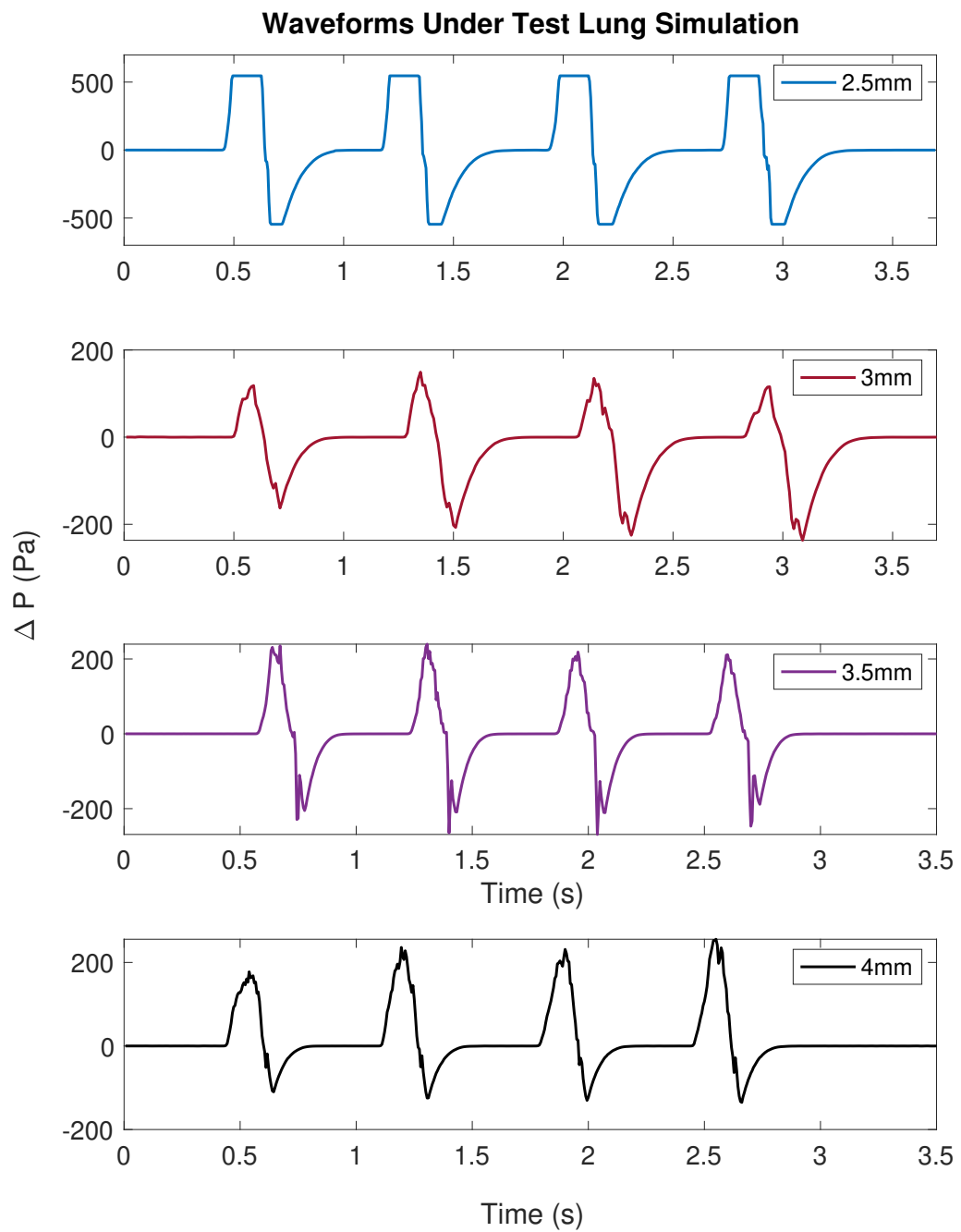


Figure 5.8: Wave-forms for all Prototypes Under Test Lung Simulation

5.6 Computational Fluid Dynamics

It was found that all designs expressed a peak pneumatic resistance significantly below the ISO 10651-4 limit of 500Pa. Resistance was assessed via static pressure that revealed peak values of 207.6, 223.983, 197.236 and 170.991 Pa for the 2.5, 3, 3.5 and 4mm designs respectively. A plot of the static pressure for the 2.5mm and 3.5mm after 100 iterations is as below, with contours reflecting those presented by Calderón et al.:

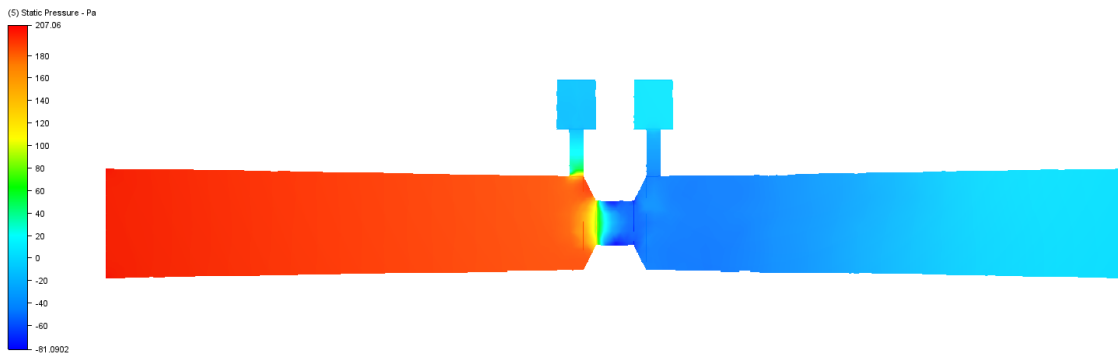


Figure 5.9: Computational Fluid Dynamics: Static Pressure at 5L/min (2.5mm)

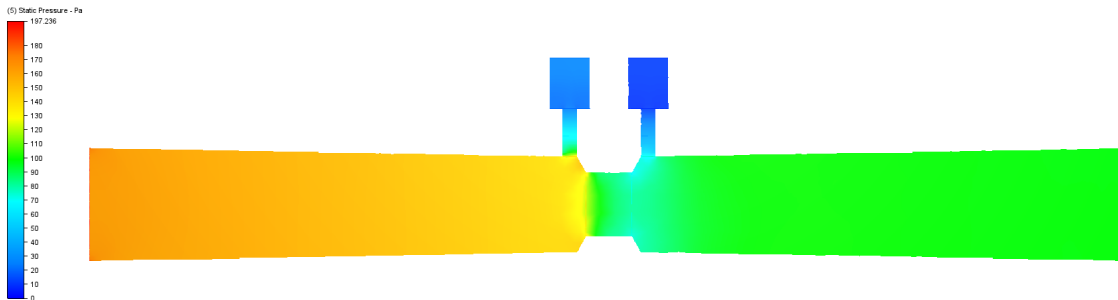


Figure 5.10: Computational Fluid Dynamics: Static Pressure at 5L/min (3.5mm)

As the size of the orifice increases we can see that the pneumatic resistance decreases as expected. However, there is an anomaly for the 3mm, reporting the highest value at a peak resistance of 223.98 Pa at the proximal connection port.

We can also see the functioning of the fixed orifice design working as expected with peak resistances measured normal to flow and a large drop in pressure following the constriction.

The differential pressure between sensor ports can also be observed, validating the working principle of fixed orifice pneumotachographs.

Additionally, an assessment of how fluid velocity behaves under these conditions was also assessed. Below is the result of the simulation on the 3.5mm design with all designs reflecting similar profiles.

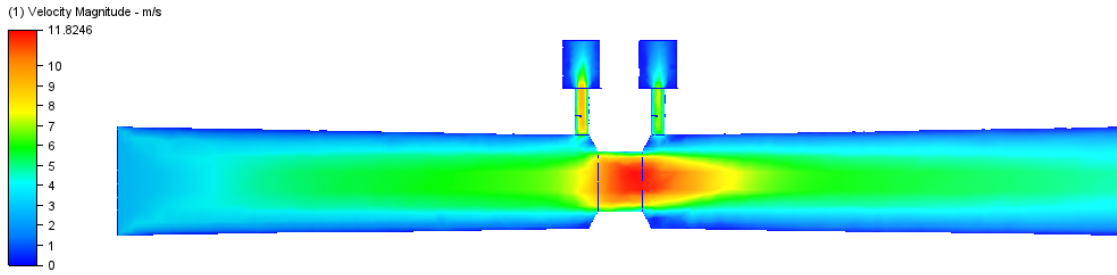


Figure 5.11: Computational Fluid Dynamics: Velocity Magnitude (3.5mm)

It can be seen that the orifice plate 'squeezes' the flow as it passes through the opening, increasing its velocity at the cost of reducing outlet pressure. Gas velocity through the proximal sensing port is also observed, with a velocity of approximately 7m/s entering this region where the sensor sits. Finally, through volumetric analysis, dead space was also obtained. This was measured as the internal volume of each design. Clearly, the trend is that smaller constrictions reduce internal volumes and therefore dead space, however, this was only a minimal reduction. A summary is as below:

Size (mm)	Dead Space (mL)	Resistance (Pa)
2.5	1.37	207.60
3.0	1.38	223.98
3.5	1.39	197.24
4.0	1.40	170.99

Table 5.4: Summary of Dead Space and Peak Pneumatic Resistance for Each Prototype

Chapter 6

Discussion

These results show that it is possible to develop a pneumotachograph tuned to the specific constraints of neonatal ventilation. Figure 5.1 and figure 5.3 present calibration curves that can inform pneumotachograph design, where orifice size can be varied dependent on the need to balance sensitivity and operating range.

This thesis designed a low cost flow sensor that can now be utilised in respiratory function monitors to assist neonatal ventilation or assess neonatal respiratory health. Studies suggest that neonatal flow rates, on average, range between \pm 4-8 L/min [47] [76]. All tested flow elements had an operating range to account for such an average. However, with differing lung compliance and the full spectrum of infant physiology, a larger flow range should ideally be implemented. Moreover, this study focused on the self inflating bag as the predominant mechanism for ventilation, due to their widespread adoption and low burden on resources. For integration into other pneumatic devices, like t-piece resuscitators, this flow range would need to be higher []. Additionally, the ability to record harmful spikes in flow was deemed necessary to flag potential injurious volumes at the time of resuscitation. From this, an aim was set to design a pneumotachograph with an operating range of at least \pm 15 slm. In regards to this, only the 3.5mm and 4mm passed, with maximum sensed flows of 16.82 and 25.32 slm respectively.

In their experimental assessment of an orifice flowmeter, Tardi et al. implement a flap in the middle of the passage that enlarges as the flowrate increases, becoming a variable orifice [68]. From this, resistance of the orifice is constant with flowrate and the relationship between differential pressure and flow becomes linear. Whilst linearizing techniques like this were avoided in this thesis due to complexity, cost and fragility, Tardi et al. suggest that they can achieve wider measurement ranges and improved calibration accuracy, two predominant concerns of this thesis. However, the researchers also note that such a variable orifice can come at the cost of dynamic properties, evident in their constant sensitivity of only $5.306 \text{ Pa/Lmin}^{-1}$, less than any of the tested devices in this analysis.

An assessment of the error against a controlled flow analyser produced results very similar to those of Edmunds et al. when they developed a flow sensor for use in low cost spirometry [78]:

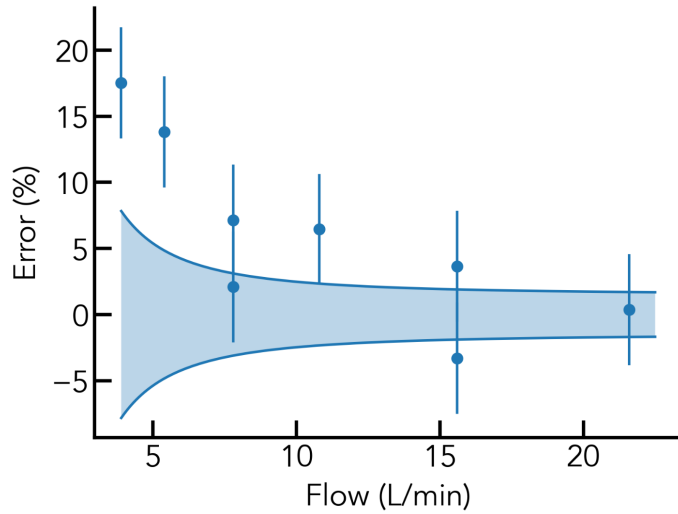


Figure 6.1: Error Against Measured Flow in a Low Cost Flow Sensor Designed by Edmunds et al. [78]

The error was lower at each mark for our 3, 3.5 and 4mm orifice designs. However, it is important to note that the flow sensor from Edmunds et al. had a much larger operating range (approximately $\pm 80\text{L/min}$). Therefore, their design traded accuracy at low flows for the higher operating range demanded by their use case. However, the American Thoracic

Society and the European Respiratory Society both state that the maximum permissible error for spirometric equipment is only $\pm 2.5\%$, of which only the 3mm passes at low flows and the 4mm passes at high flows. Edmunds et al. deliberate that if accuracy is essential, the use of two sensors could possibly be used. One for low flow accuracy and one for high flow. However, this would effectively double both cost and dead space, two elements that cannot be inflated for neonatal medicine in low-income environments.

The influence of the apparatus on pneumatic resistance and therefore the influence on infant respiratory mechanics is an important focus in the design of a pneumotachograph [58] [81]. By increasing the resistive work of breathing for a neonate, by incorporating pneumatic resistance in their breathing circuit, you may increase the energy demands of potentially critically ill patients [82]. To address such concerns ISO 10651-4 states that the pressure generated at the patient connection port must be less than 0.5 kPa at a flow of 5 L/min. By assessing this through computational fluid dynamics, it was proven that all designs were below the specified limit with the 4mm orifice generating a peak resistance of only 170.99 Pa. Moreover, this is also not at the patient connect port but at the connection port where the flow element meets other pneumatic equipment. In reality, the pressure at the connection port will most often be less than the tested value. Finally, Dead Space was between 1.37-1.40 mL for all designs, well below the limits stated by ISO 10651-4 or suggested by Pearsall et al. [56]. This value is competitive against current commercially available pneumotachometers, with the the Florian (Acturonics) and the Novametrix (Philips Respironics) having a dead space of 1ml [61]. Moreover, the length of the sensor was set to accompany an oversized breakout board used for this study. If a custom made PCB was designed, the length of the flow element could be effectively reduced, and the dead space minimised even further. photo??

6.1 Selection of the Best Pneumotachograph

In selecting the best pneumotachograph based on our particular use case, the above discussion can be utilised. Only the 3.5 and 4mm met our pre-defined operating range of ± 15 slm. Re-plotting figure 5.1 between 0 - 5 slm we can see that the 4 mm orifice may have

poor dynamic responses at low flows with a relatively flat curve that cannot sense values below 1.515 slm:

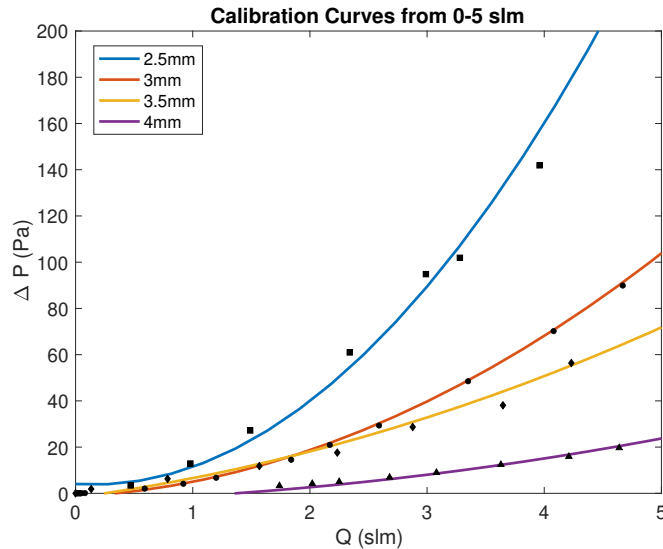


Figure 6.2: Calibration curve at low flows (0-5slm)

With both the 3.5 and 4mm showing very similar results when assessing their bidirectional nature (5.94 vs 5.32 RMSE) it would suggest a selection toward the 3.5 mm as the best performing for our particular use case. However, when each flow element was calibrated and the error in their flow measurements assessed against a control, the 3.5mm was the worst when compared to the 3 and 4mm designs. Moreover, under simulation with a test lung, portrayed in figure 5.7, we can see that the 3.5mm expressed additional noise at peak flows compared to the 4mm. These anomalies go against the trend and suggest the incorporation of manufacturing defects as discussed in following sections. However, based purely on the results of this study, the 4mm fixed orifice pneumotachograph can be seen to possess the most optimal characteristics for neonatal ventilation.

6.2 Measurement Error

Differential pressure based pneumotachometers rely on the accuracy of Bernoulli's principle for reliable flow measurement over time. It is well known that the reliability of the Bernoulli

principle erodes under heavily turbulent conditions [1]. This can be seen in our study by observing the behaviour of the 2.5mm orifice. It displayed a large difference between inspiratory and expiratory flow (RMSE 254.12Pa) and had the largest error and uncertainty at low flows (the region in which it is meant to be the most sensitive). This suggests that the small constriction is restricting the passage of flow too much and introducing unwanted turbulence, and thus, certainty in measurements. Interestingly, the 3mm did not express this problem, exhibiting great bidirectional behaviour (RMSE 29.49Pa) and low error across its operating range. This suggests that it may be the tipping point where an appropriate Reynolds number (<2000) is achieved, reducing the influence of the orifice on measurement error. However, further investigations through in depth computational fluid dynamics would need to be done to confirm this inference.

In this same way, our theoretical estimate of the calibration curves also does not account for turbulent conditions. Trettel stipulates that to extend Bernoulli's equation to more general contexts, coefficients for turbulent kinetic energy and therefore overall loss must be introduced [83]. The principle deviation from Bernoulli's principle is summarised as follows:

$$\text{loss} = \Delta\bar{k} + \frac{\rho}{m} \int_{\nabla} (\epsilon_m + \epsilon) d\nabla \quad (6.1)$$

For $\Delta\bar{k}$, the mean flow energy converted into turbulent kinetic energy and $\frac{\rho}{m} \int_{\nabla} (\epsilon_m + \epsilon) d\nabla$ the energy dissipated by mean flow (ϵ_m) and turbulence (ϵ).

Jithish et al. took similar loss terms and applied them to fixed orifice systems under CFD in simulation [84]. The study found that this, along with wall smoothness and plate thickness, dramatically influenced the coefficient of discharge and therefore the theoretical estimate of such a system's response to flow. Overall, this suggests that the lossless form of Bernoulli's equation, like in equation 2.4, can not be used to accurately model the behaviour of fixed orifice pneumotachographs. Therefore, the theoretical estimate in this thesis is deemed too rudimentary. If the ability to numerically define these systems is desired, more work has to be done to appropriately model their behaviour.

Further to this, Bernoulli's equation is dependant on the geometry of the pneumota-

chometer. In our study, a tougher resin was selected to attempt to enforce precision and consistency to the designed geometries [58]. However, the nature of SLA 3D printing is that surface smoothness, conformity to shape and overall tolerances are traded for fast prototyping. Whilst samples were cleaned in IPA, through-holes tapped again with a larger drill bit post fabrication, and inspected for any major deformities, minor defects in the fabrication would have been introduced. This can be seen in small cracks in the connectors from the removal of supports after 3D printing that may have incorporated unwanted turbulence or leak in the system. Whilst the impact of this is unknown, testing the pneumatic connectors through more formal pressure decay testing may help validate components in future work [85].



Figure 6.3: 3D-Printing Defects

Further to this, calibration happened the day of fabrication but due to the pandemic, testing was performed weeks after. Changes to geometry over time could have occurred between calibration and testing, where swelling or the loss of burrs may have influenced error measurements. In their development of a multi-patient respiratory monitor, Bourrianne et al. describe the influence of machining defects on flow calibration [86]. It can be seen that different prints from the same design expressed different calibration curves, attributed to

small defects from fabrication.

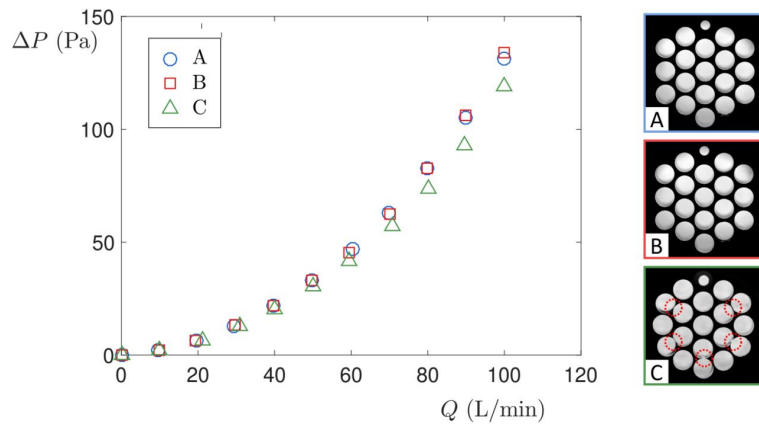


Figure 6.4: Calibration of the flow sensor for the Princeton Open Ventilation Monitor with Observed Defects [86]

To best address this, researchers CNC milled medical grade Delrin Acetal resin to produce their flow element, a tough material commonly used in FDA approved medical devices. The team then performed frozen CO₂ deburring to further remove inconsistencies:

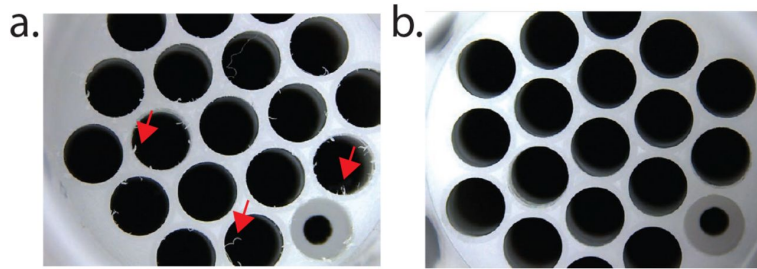


Figure 6.5: a. before and b. after frozen CO₂ deburring [86]

For future development, if the flow element needs to be commercialised at scale, the material needs to be consistent so that one single calibration curve can be produced for all manufactured elements. This can be through injection molding or CNC milling medical grade plastics, known to have more precise surface qualities.

6.3 Error in Experimental Setup

In assessing our designs ability to accurately sense flow, too significant experimental error was introduced to perform this with confidence. This error was due to inconsistent fabrication processes as listed above as well as a scarcity of correct tooling available during the COVID-19 Pandemic.

The first test, in profiling differential pressure vs flow, was performed on equipment not suited to research appropriate calibration. Whilst the Juno Training Monitor, used as the flow analyser, has a low degree of error ($\pm 0.05slm$), it is not traceable or currently CSA, CE or FDA compliant. Additionally, the screw valve on the canisters regulator, used to open and close flow, was loose and inconsistent, potentially introducing unwanted turbulence at the time of calibration.

Bourrianne et al. used an Alicat Scientific MCR-100SLPM-D mass flow controller for flow sensor calibration [86]. This allowed them to perform a controlled sweep across successive steps of flow to minimise human error. Additionally, this method collected evenly spaced data points that can be assessed as comparative pairs when evaluating differences between devices.

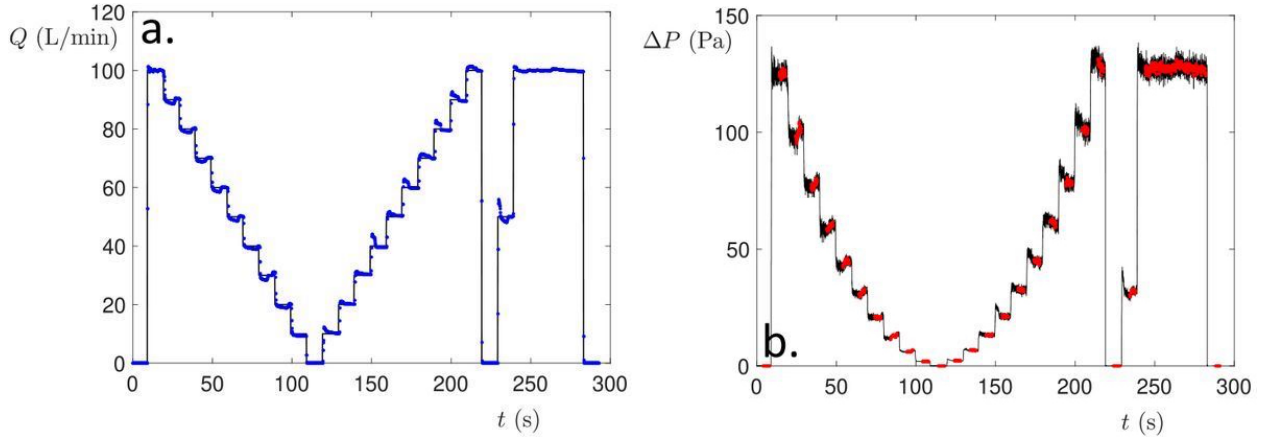


Figure 6.6: Calibration of the flow sensor for the Princeton Open Ventilation Monitor [86]

From equation 2.4, we can assess that the successful use of Bernoulli's principle to describe the transduction between differential pressure and flow relies both on the viscosity and density of the underlying gas. In this way, calibrated conditions rely on gas composition, humidity and temperature. All these factors were maintained as consistent at the time of calibration. However, the heating and humidification of inspired gases in the delivery room is often performed to avoid the complications of inhaling cold, dry air [82][87]. This is usually performed by passing inspiratory gases over a heated humidification chamber, which Fassassi et al. states should be at 37°C with an absolute humidity of 40 mgH₂O/l [88]. Whilst this is often not performed in low resource settings due to a lack of infrastructure, it is important to test sensor sensitivity under a variety of conditions. In this way, Tardi et al. assessed the influence of water vapor condensation on the performances of their orifice flowmeter [68]. They passed flow over a heated wire humidifier to produce gas up to 100% relative humidity. Researchers performed 4 hours of total testing to understand the impact of condensation build up on sensor output. Whilst results of their study showed that the formation of condensation caused a relatively negligible change in sensor sensitivity, tests still need to be done to validate this prototype under similar conditions.

6.4 Cost

A predominant aim of this thesis was to reduce costs for resource poor settings. An estimate of the final cost of the prototype is as below:

Component	Source	Cost (\$AUD)
SDP31	Digikey (300pcs)	27.01
ESP32	AliExpress	5.52
3D printing Resin	FormLabs	5.00
	Total	37.53

Table 6.1: Cost Summary

6.5 Conclusion and Future Work

A fixed orifice flow meter was designed for neonatal respiratory monitoring. Results indicate that orifice diameter greatly influences the sensitivity, bidirectionality, accuracy and pneumatic resistance of a uni-capillary sensor. This study found that a 4mm orifice performs best under the circumstances specific to neonatal ventilation. Due to the possibility of measurement and experimental error, further tests need to be performed to validate this inference. Calibration needs to be performed on traceable equipment for accurate characterisation. Additionally, further tests need to be performed to determine the deterioration of the sensor under changing conditions such as environments of increased temperature and humidity. Following this, next steps could see the commercialisation of a low cost flow sensor. This may involve advancing manufacturing to build precise flow elements out of medical grade plastics, develop custom PCBs to further miniaturise the device and design mechanisms to attach or detach sensors.

Additionally, the methodology of this study could be utilised to design a variety of low-cost flow measurement systems. Geometries can be attenuated to meet the demands of adult ventilation, where the demand for low cost solutions has surged due to overworked medical systems amidst the pandemic. Finally, as studied in the literature review, an impact outcome that can now be addressed is the development of low cost respiratory function monitors. It is suggested that by injection molding the flow elements of this study, integrating differential pressure sensors on custom PCBs, acquiring low-consumption batteries and integrating minimal LED displays, that a low cost RFM could be produced for the domains in which their need is greatest. This can be taken as a significant step forward in the development of low-cost respiratory function monitors.

Bibliography

- [1] S. N. Wall, A. C. Lee, S. Niermeyer, M. English, W. J. Keenan, W. Carlo, Z. A. Bhutta, A. Bang, I. Narayanan, I. Ariawan, and J. E. Lawn, “Neonatal resuscitation in low-resource settings: What, who, and how to overcome challenges to scale up?” in *International Journal of Gynecology and Obstetrics*, vol. 107, no. SUPPL. John Wiley and Sons Ltd, 2009.
- [2] J. E. Lawn, S. Cousens, and J. Zupan, “4 Million neonatal deaths: When? Where? Why?” pp. 891–900, 3 2005. [Online]. Available: <https://pubmed.ncbi.nlm.nih.gov/15752534/>
- [3] S. N. Wall, A. C. Lee, W. Carlo, R. Goldenberg, S. Niermeyer, G. L. Darmstadt, W. Keenan, Z. A. Bhutta, J. Perlman, and J. E. Lawn, “Reducing Intrapartum-Related Neonatal Deaths in Low- and Middle-Income Countries—What Works?” pp. 395–407, 12 2010.
- [4] A. Al Balushi, M. A. L. Laporte, and P. Wintermark, “The Impact of Ventilation on the Development of Brain Injury in Asphyxiated Newborns Treated with Hypothermia,” in *Respiratory Management of Newborns*. InTech, 8 2016. [Online]. Available: <http://dx.doi.org/10.5772/63385>
- [5] S. Zhang, B. Li, X. Zhang, C. Zhu, and X. Wang, “Birth Asphyxia Is Associated With Increased Risk of Cerebral Palsy: A Meta-Analysis,” *Frontiers in Neurology*, vol. 11, p. 704, 7 2020. [Online]. Available: [/pmc/articles/PMC7381116//pmc/articles/PMC7381116/?report=abstract](https://www.ncbi.nlm.nih.gov/pmc/articles/PMC7381116/?report=abstract)

BIBLIOGRAPHY

- [6] R. Moshiro, P. Mdoe, and J. M. Perlman, “A Global View of Neonatal Asphyxia and Resuscitation,” p. 489, 11 2019. [Online]. Available: [/pmc/articles/PMC6902004//pmc/articles/PMC6902004/?report=abstract](https://www.ncbi.nlm.nih.gov/pmc/articles/PMC6902004/)<https://www.ncbi.nlm.nih.gov/pmc/articles/PMC6902004/>
- [7] J. L. Wallander, C. Bann, E. Chomba, S. S. Goudar, O. Pasha, F. J. Biasini, E. M. McClure, V. Thorsten, D. Wallace, and W. A. Carlo, “Developmental trajectories of children with birth asphyxia through 36months of age in low/low-middle income countries,” *Early Human Development*, vol. 90, no. 7, pp. 343–348, 2014. [Online]. Available: [/pmc/articles/PMC4097313//pmc/articles/PMC4097313/?report=abstract](https://www.ncbi.nlm.nih.gov/pmc/articles/PMC4097313/)<https://www.ncbi.nlm.nih.gov/pmc/articles/PMC4097313/>
- [8] D. R. Halloran, E. McClure, H. Chakraborty, E. Chomba, L. L. Wright, and W. A. Carlo, “Birth asphyxia survivors in a developing country,” *Journal of Perinatology*, vol. 29, no. 3, pp. 243–249, 2009. [Online]. Available: [/pmc/articles/PMC3807866//pmc/articles/PMC3807866/?report=abstract](https://www.ncbi.nlm.nih.gov/pmc/articles/PMC3807866/)<https://www.ncbi.nlm.nih.gov/pmc/articles/PMC3807866/>
- [9] C. M. Robertson, N. N. Finer, and M. G. Grace, “School performance of survivors of neonatal encephalopathy associated with birth asphyxia at term,” *The Journal of Pediatrics*, vol. 114, no. 5, pp. 753–760, 5 1989. [Online]. Available: <http://www.jpeds.com/article/S0022347689801325/fulltext><http://www.jpeds.com/article/S0022347689801325/abstract>[https://www.jpeds.com/article/S0022-3476\(89\)80132-5/abstract](https://www.jpeds.com/article/S0022-3476(89)80132-5/abstract)
- [10] C. P. O'Donnell, C. O. Kamlin, P. G. Davis, and C. J. Morley, “Neonatal resuscitation 1: A model to measure inspired and expired tidal volumes and assess leakage at the face mask,” *Archives of Disease in Childhood: Fetal and Neonatal Edition*, vol. 90, no. 5, p. F388, 9 2005. [Online]. Available: www.archdischild.com
- [11] “Neonatal Resuscitation Education Program - NeoResus — Improvement Exchange — Clinical Excellence Queensland — Queensland Health.”

BIBLIOGRAPHY

- [Online]. Available: <https://clinicalexcellence.qld.gov.au/improvement-exchange/neonatal-resuscitation-education-program-neoresus>
- [12] M. Hinder and M. Tracy, "Newborn resuscitation devices: The known unknowns and the unknown unknowns," *Seminars in Fetal and Neonatal Medicine*, vol. 26, no. 2, p. 101233, 4 2021.
- [13] "UN Commission on Life-Saving Commodities for Women and Children — UNFPA - United Nations Population Fund." [Online]. Available: <https://www.unfpa.org/publications/un-commission-life-saving-commodities-women-and-children>
- [14] "WHO — Guidelines on basic newborn resuscitation," *WHO*, 2019. [Online]. Available: http://www.who.int/maternal_child_adolescent/documents/basic_newborn_resuscitation/en/
- [15] "Difference in Manual Ventilation: Self-Inflating Ventilation Bag vs. a Free Flow Inflating Bag - The Airway Jedi." [Online]. Available: <https://airwayjedi.com/2017/03/26/manual-ventilation-self-inflating-vs-free-flow-bag/>
- [16] A. Khoury, S. Hugonnot, J. Cossus, A. De Luca, T. Desmettre, F. S. Sall, and G. Capellier, "From mouth-to-mouth to bag-valve-mask ventilation: Evolution and characteristics of actual devices - A review of the literature," 2014.
- [17] M. B. Tracy, R. Halliday, S. K. Tracy, and M. K. Hinder, "Newborn self-inflating manual resuscitators: Precision robotic testing of safety and reliability," *Archives of Disease in Childhood: Fetal and Neonatal Edition*, vol. 104, no. 4, pp. F403–F408, 7 2019.
- [18] D. N. Carbone, N. N. Finer, E. Knodel, and W. Rich, "Video recording as a means of evaluating neonatal resuscitation performance," *Pediatrics*, vol. 106, no. 4 I, pp. 654–658, 2000. [Online]. Available: <https://pubmed.ncbi.nlm.nih.gov/11015505/>
- [19] T. A. Katz, D. D. Weinberg, C. E. Fishman, V. Nadkarni, P. Tremoulet, A. B. Te Pas, A. Sarcevic, and E. E. Foglia, "Visual attention on a respiratory function monitor during simulated neonatal resuscitation: An eye-tracking study," *Archives of Disease*

BIBLIOGRAPHY

- in Childhood: Fetal and Neonatal Edition*, vol. 104, no. 3, 5 2019. [Online]. Available: <https://pubmed.ncbi.nlm.nih.gov/29903721/>
- [20] E. O'currain, M. Thio, J. A. Dawson, S. M. Donath, P. G. Davis, and O. . Curraín, “Respiratory monitors to teach newborn facemask ventilation: a randomised trial.” [Online]. Available: <http://fn.bmj.com/>
- [21] G. M. Schmölzer and C. C. Roehr, “Use of respiratory function monitors during simulated neonatal resuscitation,” pp. 261–266, 2011.
- [22] D. Jain, C. D'Ugard, A. Aguilar, T. Del Moral, E. Bancalari, and N. Claure, “Use of a mechanical ventilator with respiratory function monitoring provides more consistent ventilation during simulated neonatal resuscitation,” *Neonatology*, vol. 117, no. 2, pp. 151–158, 7 2020. [Online]. Available: <https://www.karger.com/Article/FullText/503257> <https://www.karger.com/Article/Abstract/503257>
- [23] F. E. Wood, C. J. Morley, J. A. Dawson, and P. G. Davis, “A respiratory function monitor improves mask ventilation,” *Archives of Disease in Childhood: Fetal and Neonatal Edition*, vol. 93, no. 5, 9 2008. [Online]. Available: <https://pubmed.ncbi.nlm.nih.gov/18192329/>
- [24] C. D. Lilley, M. Stewart, and C. J. Morley, “Respiratory function monitoring during neonatal emergency transport,” *Archives of Disease in Childhood: Fetal and Neonatal Edition*, vol. 90, no. 1, pp. 82–83, 1 2005. [Online]. Available: <http://fn.bmj.com/>
- [25] S. U. Morton and D. Brodsky, “Fetal Physiology and the Transition to Extrauterine Life,” pp. 395–407, 9 2016. [Online]. Available: <https://europepmc.org/articles/PMC4987541> <https://europepmc.org/article/pmc/4987541>
- [26] F. H. A. MARSHALL, “Researches on Pre-Natal Life,” *Nature*, vol. 159, no. 4038, pp. 383–384, 3 1947. [Online]. Available: <https://www.nature.com/articles/159383a0>
- [27] T. A. Roberts, J. F. van Amerom, A. Uus, D. F. Lloyd, M. P. van Poppel, A. N. Price, J. D. Tournier, C. A. Mohanadass, L. H. Jackson, S. J. Malik, K. Pushparajah, M. A.

BIBLIOGRAPHY

- Rutherford, R. Rezavi, M. Deprez, and J. V. Hajnal, “Fetal whole heart blood flow imaging using 4D cine MRI,” *Nature Communications*, vol. 11, no. 1, pp. 1–13, 12 2020. [Online]. Available: <https://doi.org/10.1038/s41467-020-18790-1>
- [28] C. M. J. Tan and A. J. Lewandowski, “The Transitional Heart: From Early Embryonic and Fetal Development to Neonatal Life,” pp. 373–386, 5 2020. [Online]. Available: www.karger.com/fdt
- [29] A. Finnemore and A. Groves, “Physiology of the fetal and transitional circulation,” pp. 210–216, 8 2015. [Online]. Available: <https://pubmed.ncbi.nlm.nih.gov/25921445/>
- [30] A. Gupta and A. Paria, “Transition from fetus to neonate,” pp. 593–596, 12 2016.
- [31] N. H. Hillman, S. G. Kallapur, and A. H. Jobe, “Physiology of transition from intrauterine to extrauterine life,” pp. 769–783, 12 2012. [Online]. Available: [/pmc/articles/PMC3504352//pmc/articles/PMC3504352/?report=abstract](https://pmc/articles/PMC3504352//pmc/articles/PMC3504352/?report=abstract)<https://www.ncbi.nlm.nih.gov/pmc/articles/PMC3504352/>
- [32] M. F. Lutfi, “The physiological basis and clinical significance of lung volume measurements,” *Multidisciplinary Respiratory Medicine*, vol. 12, no. 1, pp. 1–12, 2 2017. [Online]. Available: <https://mrmjournal.biomedcentral.com/articles/10.1186/s40248-017-0084-5>
- [33] R. E. Olver, D. V. Walters, and S. M. Wilson, “Developmental regulation of lung liquid transport,” pp. 77–101, 2004. [Online]. Available: <https://pubmed.ncbi.nlm.nih.gov/14977397/>
- [34] S. B. Hooper, M. J. Kitchen, M. J. Wallace, N. Yagi, K. Uesugi, M. J. Morgan, C. Hall, K. K. W. Siu, I. M. Williams, M. Siew, S. C. Irvine, K. Pavlov, and R. A. Lewis, “Imaging lung aeration and lung liquid clearance at birth,” *The FASEB Journal*, vol. 21, no. 12, pp. 3329–3337, 10 2007. [Online]. Available: <https://faseb.onlinelibrary.wiley.com/doi/full/10.1096/fj.07-8208com>
<https://faseb.onlinelibrary.wiley.com/doi/abs/10.1096/fj.07-8208com>
<https://faseb.onlinelibrary.wiley.com/doi/10.1096/fj.07-8208com>

BIBLIOGRAPHY

- [35] M. E. Probyn, M. J. Wallace, and S. B. Hooper, "Effect of increased lung expansion on lung growth and development near midgestation in fetal sheep," *Pediatric Research*, vol. 47, no. 6, pp. 806–812, 2000. [Online]. Available: <https://www.nature.com/articles/pr2000138>
- [36] P. M. Barker and R. E. Olver, "Invited review: Clearance of lung liquid during the perinatal period," *Journal of Applied Physiology*, vol. 93, no. 4, pp. 1542–1548, 2002. [Online]. Available: <http://www.jap.org>
- [37] R. D. Bland, "Loss of liquid from the lung lumen in labor: More than a simple 'squeeze,'" 2001. [Online]. Available: <http://www.ajplung.org>
- [38] A. B. te Pas, P. G. Davis, S. B. Hooper, and C. J. Morley, "From Liquid to Air: Breathing after Birth," *Journal of Pediatrics*, vol. 152, no. 5, pp. 607–611, 5 2008.
- [39] A. D. Milner and R. A. Saunders, "Pressure and volume changes during the first breath of human neonates," *Archives of Disease in Childhood*, vol. 52, no. 12, pp. 918–924, 1977. [Online]. Available: [/pmc/articles/PMC1545011/?report=abstract](https://pmc/articles/PMC1545011/?report=abstract) <https://www.ncbi.nlm.nih.gov/pmc/articles/PMC1545011/>
- [40] A. B. Te Pas, C. Wong, C. O. F. Kamlin, J. A. Dawson, C. J. Morley, and P. G. Davis, "Breathing patterns in preterm and term infants immediately after birth," *Pediatric Research*, vol. 65, no. 3, pp. 352–356, 3 2009. [Online]. Available: <https://www.nature.com/articles/pr200967>
- [41] S. B. Hooper and R. Harding, "FETAL LUNG LIQUID: A MAJOR DETERMINANT OF THE GROWTH AND FUNCTIONAL DEVELOPMENT OF THE FETAL LUNG," *Clinical and Experimental Pharmacology and Physiology*, vol. 22, no. 4, pp. 235–241, 1995. [Online]. Available: <https://pubmed.ncbi.nlm.nih.gov/7671435/>
- [42] L. Jain and D. C. Eaton, "Physiology of fetal lung fluid clearance and the effect of labor," in *Seminars in Perinatology*, vol. 30, no. 1. Semin Perinatol, 2 2006, pp. 34–43. [Online]. Available: <https://pubmed.ncbi.nlm.nih.gov/16549212/>

BIBLIOGRAPHY

- [43] O. D. Saugstad, N. J. Robertson, and M. Vento, “A critical review of the 2020 International Liaison Committee on Resuscitation treatment recommendations for resuscitating the newly born infant,” *Acta Paediatrica, International Journal of Paediatrics*, vol. 110, no. 4, pp. 1107–1112, 4 2021. [Online]. Available: <https://onlinelibrary.wiley.com/doi/full/10.1111/apa.15754>
- [44] J. Kattwinkel, C. Stewart, B. Walsh, M. Gurka, and A. Paget-Brown, “Responding to compliance changes in a lung model during manual ventilation: Perhaps volume, rather than pressure, should be displayed,” *Pediatrics*, vol. 123, no. 3, 3 2009. [Online]. Available: <https://pubmed.ncbi.nlm.nih.gov/19188267/>
- [45] C. P. O’Donnell, P. G. Davis, R. Lau, P. A. Dargaville, L. W. Doyle, and C. J. Morley, “Neonatal resuscitation 2: An evaluation of manual ventilation devices and face masks,” *Archives of Disease in Childhood: Fetal and Neonatal Edition*, vol. 90, no. 5, 9 2005. [Online]. Available: <https://pubmed.ncbi.nlm.nih.gov/15871989/>
- [46] G. M. Schmölzer, J. A. Dawson, C. O. F. Kamlin, C. P. O’Donnell, C. J. Morley, and P. G. Davis, “Airway obstruction and gas leak during mask ventilation of preterm infants in the delivery room,” *Archives of Disease in Childhood: Fetal and Neonatal Edition*, vol. 96, no. 4, 7 2011.
- [47] T. Martherus, A. Oberthuer, J. Dekker, S. B. Hooper, E. V. Mcgillick, A. Kribs, and A. B. Te Pas, “Supporting breathing of preterm infants at birth: a narrative review.” [Online]. Available: <http://fn.bmjjournals.org/>
- [48] G. M. Schmölzer, C. J. Morley, C. Wong, J. A. Dawson, C. O. F. Kamlin, S. M. Donath, S. B. Hooper, and P. G. Davis, “Respiratory function monitor guidance of mask ventilation in the delivery room: A feasibility study,” *Journal of Pediatrics*, vol. 160, no. 3, 2012.
- [49] S. M. Hartmann, R. W. Farris, J. L. Di Gennaro, and J. S. Roberts, “Systematic review and meta-analysis of end-tidal carbon dioxide values

BIBLIOGRAPHY

- associated with return of spontaneous circulation during cardiopulmonary resuscitation,” *Journal of Intensive Care Medicine*, vol. 30, no. 7, pp. 426–435, 10 2015. [Online]. Available: https://journals.sagepub.com/doi/full/10.1177/0885066614530839?casa_token=m526o3WdYe8AAAAA%3AJuTcA55VPISf9QCzIc8n6b4eRTe2LvlSI3E31HEQRJ-DkgdePJabKFIjd_fZH5uhkeeYB-OcRC8vvQ
- [50] F. E. Wood, C. J. Morley, J. A. Dawson, C. O. F. Kamlin, L. S. Owen, S. Donath, and P. G. Davis, “Improved techniques reduce face mask leak during simulated neonatal resuscitation: Study 2,” *Archives of Disease in Childhood: Fetal and Neonatal Edition*, vol. 93, no. 3, 5 2008. [Online]. Available: <https://pubmed.ncbi.nlm.nih.gov/18039750/>
- [51] J. Klimek, C. J. Morley, R. Lau, and P. G. Davis, “Does measuring respiratory function improve neonatal ventilation,” *Journal of Paediatrics and Child Health*, vol. 42, no. 3, pp. 140–142, 3 2006. [Online]. Available: <https://pubmed.ncbi.nlm.nih.gov/16509915/>
- [52] M. Crott, “Neonatal Respiratory Function Monitoring in research & clinical use,” Tech. Rep.
- [53] E. Schena, G. Lupi, S. Cecchini, and S. Silvestri, “Linearity dependence on oxygen fraction and gas temperature of a novel Fleisch pneumotachograph for neonatal ventilation at low flow rates,” *Measurement: Journal of the International Measurement Confederation*, vol. 45, no. 8, pp. 2064–2071, 10 2012.
- [54] M. A, M. V, B. P, F. G, C. ME, M. AD, and G. A, “Evaluation of respiratory function monitoring at the resuscitation of prematurely born infants,” *European journal of pediatrics*, vol. 174, no. 2, pp. 205–208, 1 2015. [Online]. Available: <https://pubmed.ncbi.nlm.nih.gov/25029987/>
- [55] S. Intagliata, A. Rizzo, and W. Gossman, “Physiology, Lung Dead Space,” *StatPearls*, 10 2021. [Online]. Available: <https://www.ncbi.nlm.nih.gov/books/NBK482501/>
- [56] M. F. Pearsall and J. M. Feldman, “When does apparatus dead space matter for the pediatric patient?” *Anesthesia and Analgesia*, vol. 118, no. 4, pp. 776–780,

BIBLIOGRAPHY

2014. [Online]. Available: https://journals.lww.com/anesthesia-analgesia/Fulltext/2014/04000/When_Apparatus_Dead_Space_Matter_for_the.14.aspx
- [57] B. Y. Louis K and A. Professor, “On the convection of heat from small cylinders in a stream of fluid: Determination of the convection constants of small platinum wires, with applications to hot-wire anemometry,” *Proceedings of the Royal Society of London. Series A, Containing Papers of a Mathematical and Physical Character*, vol. 90, no. 622, pp. 563–570, 9 1914. [Online]. Available: <https://royalsocietypublishing.org/>
- [58] E. Schena, C. Massaroni, P. Saccomandi, and S. Cecchini, “Flow measurement in mechanical ventilation: A review,” pp. 257–264, 3 2015. [Online]. Available: <https://pubmed.ncbi.nlm.nih.gov/25659299/>
- [59] E. Özahi, M. Çarpinlioğlu, and M. Y. Gündoğdu, “Simple methods for low speed calibration of hot-wire anemometers,” *Flow Measurement and Instrumentation*, vol. 21, no. 2, pp. 166–170, 6 2010.
- [60] K. M. Talluru, V. Kulandaivelu, N. Hutchins, and I. Marusic, “A calibration technique to correct sensor drift issues in hot-wire anemometry,” *Measurement Science and Technology*, vol. 25, no. 10, p. 105304, 10 2014. [Online]. Available: <https://iopscience.iop.org/article/10.1088/0957-0233/25/10/105304https://iopscience.iop.org/article/10.1088/0957-0233/25/10/105304/meta>
- [61] C. Verbeek, H. A. van Zanten, J. J. van Vonderen, M. J. Kitchen, S. B. Hooper, and A. B. te Pas, “Accuracy of currently available neonatal respiratory function monitors for neonatal resuscitation,” *European Journal of Pediatrics*, vol. 175, no. 8, pp. 1065–1070, 8 2016. [Online]. Available: <https://pmc/articles/PMC4930469//pmc/articles/PMC4930469/?report=abstracthttps://www.ncbi.nlm.nih.gov/pmc/articles/PMC4930469/>
- [62] I. Yoshiya, T. Nakajima, I. Nagai, and S. Jitsukawa, “A bidirectional respiratory flowmeter using the hot wire principle,” *Journal of Applied Physiology*, vol. 38, no. 2, pp. 360–365, 1975. [Online]. Available: <https://pubmed.ncbi.nlm.nih.gov/1120766/>

BIBLIOGRAPHY

- [63] A. F. van Putten, “An integrated silicon double bridge anemometer,” *Sensors and Actuators*, vol. 4, no. C, pp. 387–396, 1 1983.
- [64] M. J. Van Putten, C. R. Kleijn, and H. E. Van Den Akker, “Multi-parameter sensing with a thermal silicon flow sensor,” *Journal of Fluids Engineering, Transactions of the ASME*, vol. 124, no. 3, pp. 643–649, 9 2002. [Online]. Available: http://asmedigitalcollection.asme.org/fluidsengineering/article-pdf/124/3/643/5901062/643_1.pdf
- [65] “CMOSens Technology for Gas Flow — Sensirion.” [Online]. Available: <https://www.sensirion.com/en/about-us/company/technology/cmosens-technology-for-gas-flow/>
- [66] C. Jacq, T. Maeder, E. Haemmerle, N. Craquelin, and P. Ryser, “Ultra-low pressure sensor for neonatal resuscitator,” in *Procedia Engineering*, vol. 5. Elsevier Ltd, 1 2010, pp. 532–535.
- [67] M. R. Miller and A. C. Pincock, “Linearity and temperature control of the Fleisch pneumotachograph,” *Journal of applied physiology (Bethesda, Md. : 1985)*, vol. 60, no. 2, pp. 710–715, 1986. [Online]. Available: <https://pubmed.ncbi.nlm.nih.gov/3949670/>
- [68] G. Tardi, C. Massaroni, P. Saccomandi, and E. Schena, “Experimental assessment of a variable orifice flowmeter for respiratory monitoring,” *Journal of Sensors*, vol. 2015, 2015.
- [69] K. E. Finucane, B. A. Egan, and S. V. Dawson, “Linearity and frequency response of pneumotachographs,” *APPLIED PHYSIOLOGY*, vol. 1, 1972.
- [70] E. Schena, G. Masselli, and S. Silvestri, “Influence of gas temperature on the performances of a low dead space capillary type pneumotachograph for neonatal ventilation,” *Proceedings of the 31st Annual International Conference of the IEEE Engineering in Medicine and Biology Society: Engineering the Future of Biomedicine, EMBC 2009*, pp. 1226–1229, 2009.
- [71] A. Giannella-Neto, C. Bellido, R. B. Barbosa, and M. F. Vidal Melo, “Design and

BIBLIOGRAPHY

- calibration of unicapillary pneumotachographs,” *Journal of Applied Physiology*, vol. 84, no. 1, pp. 335–343, 1998. [Online]. Available: <http://www.jap.org>
- [72] F. Takatori, S. Inoue, S. Togo, and S. Yamamori, “Development of respiratory function monitor for neonates,” in *Proceedings of the Annual International Conference of the IEEE Engineering in Medicine and Biology Society, EMBS*, vol. 2017. Institute of Electrical and Electronics Engineers Inc., 9 2017, pp. 3719–3722. [Online]. Available: <https://pubmed.ncbi.nlm.nih.gov/29060706/>
- [73] R. S. Khandpur, “Pneumotachometers,” in *Compendium of Biomedical Instrumentation*. Wiley, 2 2020, pp. 1561–1564. [Online]. Available: <https://onlinelibrary.wiley.com/doi/full/10.1002/9781119288190.ch295> <https://onlinelibrary.wiley.com/doi/abs/10.1002/9781119288190.ch295> <https://onlinelibrary.wiley.com/doi/10.1002/9781119288190.ch295>
- [74] “SFM3400 - Mass Flow Meter — Sensirion.” [Online]. Available: <https://www.sensirion.com/en/flow-sensors/mass-flow-meters-for-high-precise-measurement-of-gases/proximal-flow-sensor-for-neonatal-and-pediatric-applications/>
- [75] J. Calderón, C. Rincón, B. Agreda, S. Calero, M. Bornas, and J. J. J. d. Cisneros, “A Low-Cost Air Flow Sensor/Transducer for Medical Applications: Design and Experimental Characterization,” 1 2021. [Online]. Available: <https://www.preprints.org/manuscript/202101.0404/v1>
- [76] D. Trevisanuto, V. Dal Cengio, N. Doglioni, F. Cavallin, V. Zanardo, M. Parotto, and G. Weiner, “Oxygen Delivery Using a Neonatal Self-inflating Resuscitation Bag: Effect of Oxygen Flow,” *Pediatrics*, vol. 131, pp. 1144–1149, 2013. [Online]. Available: www.pediatrics.org/cgi/doi/10.1542/peds.2012-3116
- [77] BREATHNEY, “SENSOR MODULE.” [Online]. Available: <https://breathney.vub.be/sensor-module/>
- [78] J. L. Edmunds, M. J. Bustamante, D. K. Piech, J. S. Schor, S. J. Raymond, D. B.

BIBLIOGRAPHY

- Camarillo, and M. M. Maharbiz, “Low-Cost Differential Pressure Spirometry for Emergency Ventilator Tidal Volume Sensing,” 9 2020.
- [79] C. L. Hollingshead, M. C. Johnson, S. L. Barfuss, and R. E. Spall, “Discharge coefficient performance of Venturi, standard concentric orifice plate, V-cone and wedge flow meters at low Reynolds numbers,” *Journal of Petroleum Science and Engineering*, vol. 78, no. 3-4, pp. 559–566, 9 2011.
- [80] JCGM, “Evaluation of measurement data-Guide to the expression of uncertainty in measurement Évaluation des données de mesure-Guide pour l’expression de l’incertitude de mesure,” 2008. [Online]. Available: www.bipm.org
- [81] P. Vallinis, G. M. Davis, and A. L. Coates, “A very low dead space pneumotachograph for ventilatory measurements in newborns,” Tech. Rep.
- [82] A. Uchiyama, T. Yoshida, H. Yamanaka, and Y. Fujino, “Estimation of Tracheal Pressure and Imposed Expiratory Work of Breathing by the Endotracheal Tube, Heat and Moisture Exchanger, and Ventilator During Mechanical Ventilation,” *Respiratory Care*, vol. 58, no. 7, pp. 1157–1169, 7 2013. [Online]. Available: <http://rc.rcjournal.com/content/58/7/1157> <http://rc.rcjournal.com/content/58/7/1157.abstract>
- [83] B. Trettel, “Estimating turbulent kinetic energy and dissipation with internal flow loss coefficients,” *ICLASS 2018 - 14th International Conference on Liquid Atomization and Spray Systems*, 2020. [Online]. Available: <https://engrxiv.org/qsf7/>
- [84] K. S. Jithish and P. V. Ajay Kumar, “Analysis of turbulent flow through an orifice meter using experimental and computational fluid dynamics simulation approach—A case study:,” <http://dx.doi.org/10.1177/0306419015604432>, vol. 43, no. 4, pp. 233–246, 9 2015. [Online]. Available: <https://journals.sagepub.com/doi/10.1177/0306419015604432>
- [85] J. T. Mcglone, “Quantitative Respirator Fit Testing Through Dynamic Pressure Decay Measurement,” 2011. [Online]. Available: <https://www.tandfonline.com/action/journalInformation?journalCode=uaoh20>

BIBLIOGRAPHY

- [86] T. P. O. V. M. Collaboration, P. Bourrianne, S. Chidzik, D. Cohen, P. Elmer, T. Hallowell, T. J. Kilbaugh, D. Lange, A. M. Leifer, D. R. Marlow, P. D. Meyers, E. Normand, J. Nunes, M. Oh, L. Page, T. Periera, J. Pi- varska, H. Schreiner, H. A. Stone, D. W. Tank, S. Thiberge, and C. Tully, “Inexpensive multi-patient respiratory monitoring system for helmet ventilation during COVID-19 pandemic,” *medRxiv*, p. 2020.06.29.20141283, 6 2021. [Online]. Available: <https://www.medrxiv.org/content/10.1101/2020.06.29.20141283v3>
- [87] T. N. Doctor, J. P. Foster, A. Stewart, K. Tan, D. A. Todd, and L. Mcgrory, “Heated and humidified inspired gas through heated humidifiers in comparison to non-heated and non-humidified gas in hospitalised neonates receiving respiratory support,” *The Cochrane Database of Systematic Reviews*, vol. 2017, no. 2, 2 2017. [Online]. Available: [/pmc/articles/PMC6464096/](https://pmc/articles/PMC6464096/) ?report=abstract
- [88] M. Fassassi, F. Michel, L. Thomachot, C. Nicaise, R. Vialet, Y. Jammes, P. Lagier, and C. Martin, “Airway humidification with a heat and moisture exchanger in mechanically ventilated neonates: A preliminary evaluation,” *Intensive Care Medicine*, vol. 33, no. 2, pp. 336–343, 2 2007. [Online]. Available: <https://link.springer.com/article/10.1007/s00134-006-0466-1>

Appendix A

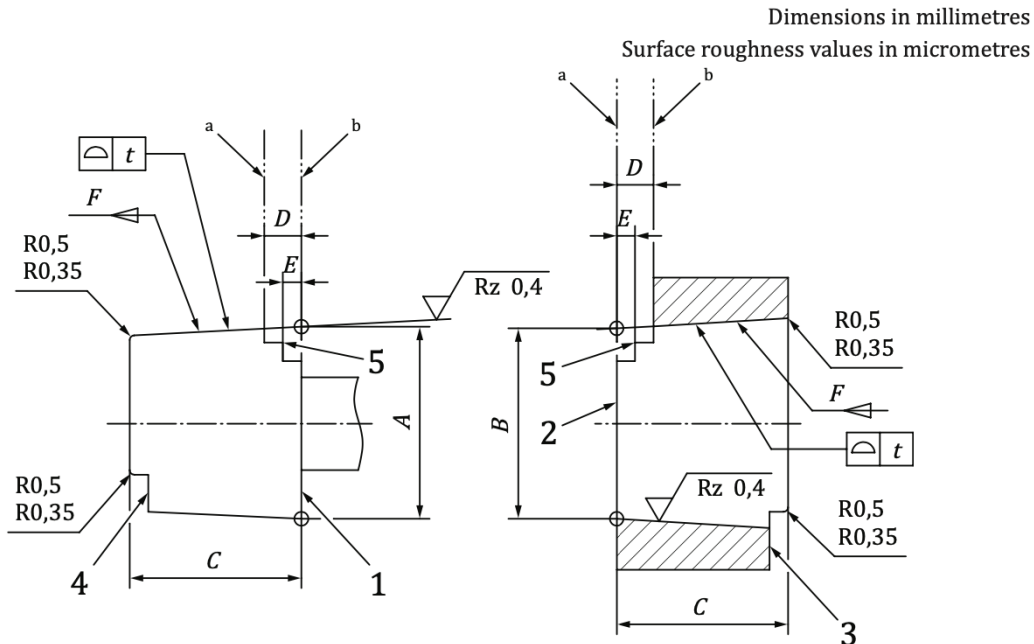
A.1 Test conditions for ventilatory performance: ISO 10651-4:2009

Patient Body mass B^a Kg	Compliance l/kPa	Resistance kPa/(l/s)	Inspiration: Expiration ratio $\pm 20\%$	Frequency f Breaths/min $\pm 10\%$	Minimum delivered volume V_{Del} ml
$B \leq 5$	0,01	40	1:1	60	20
$5 < B \leq 10$	0,1	2	1:2	25	150
$10 < B \leq 40$	0,2	2	1:2	20	$15 \times B^{1)}$
$B > 40$	0,2	2	1:2	20	600

^a B = Body mass, in kilograms, designated by the manufacturer in the manual.

Figure A.1: BS EN ISO 10651-4:2009h

A.2 Interconnecting details of cones and sockets: ISO 5356-1:2015(E)



Connector size			Taper length	Clearance to shoulder (if present)	Length to taper	Taper ratio	Minimum internal diameter of cone	Minimum length of internal diameter of the cone (G)
	A	B	C	D	E	F	G	H
8,5	$8,45 \pm 0,04$	6	$\geq 6,4$	$\geq 8,9$	≥ 8	1:19	6,25	6,0
11,5	$11,50 \pm 0,04$	10	$\geq 13,5$	≥ 16	≥ 15	1:40	a	a
15	$15,47 \pm 0,04$	10	≥ 16	≥ 16	$\geq 14,5$	1:40	a	a
22	$22,37 \pm 0,04$	15	≥ 21	See Figure 3	See Figure 3	1:40	a	a
23	$23,175 \pm 0,02$	13	≥ 18	≥ 18	≥ 15	1:36	a	a
30	$30,9 \pm 0,05$	14	≥ 18	≥ 18	≥ 14	1:20	27,0	12,0

Figure A.2: Dimensions of cones and sockets

A.3 Raw Signal From Experiment 4.7.1

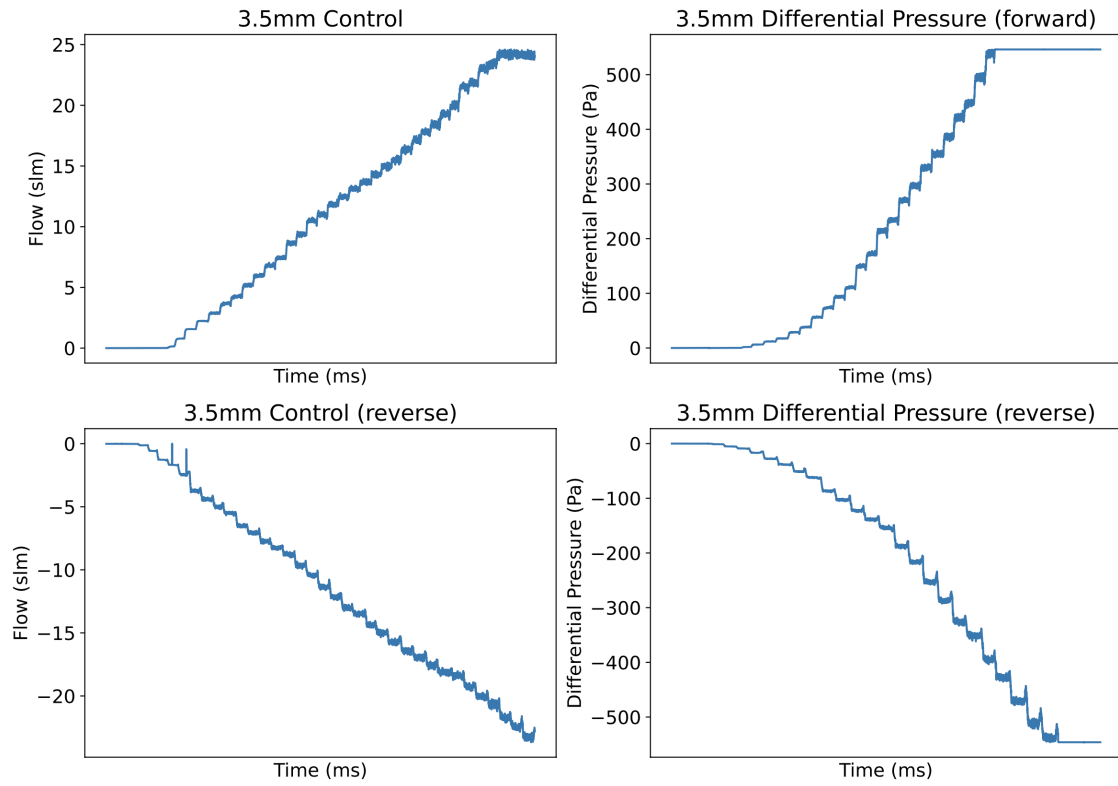


Figure A.3: Raw Signals: Differential Pressure vs Flow for 3.5mm Orifice

A.4 Image of the Test Setup for 4.7.3

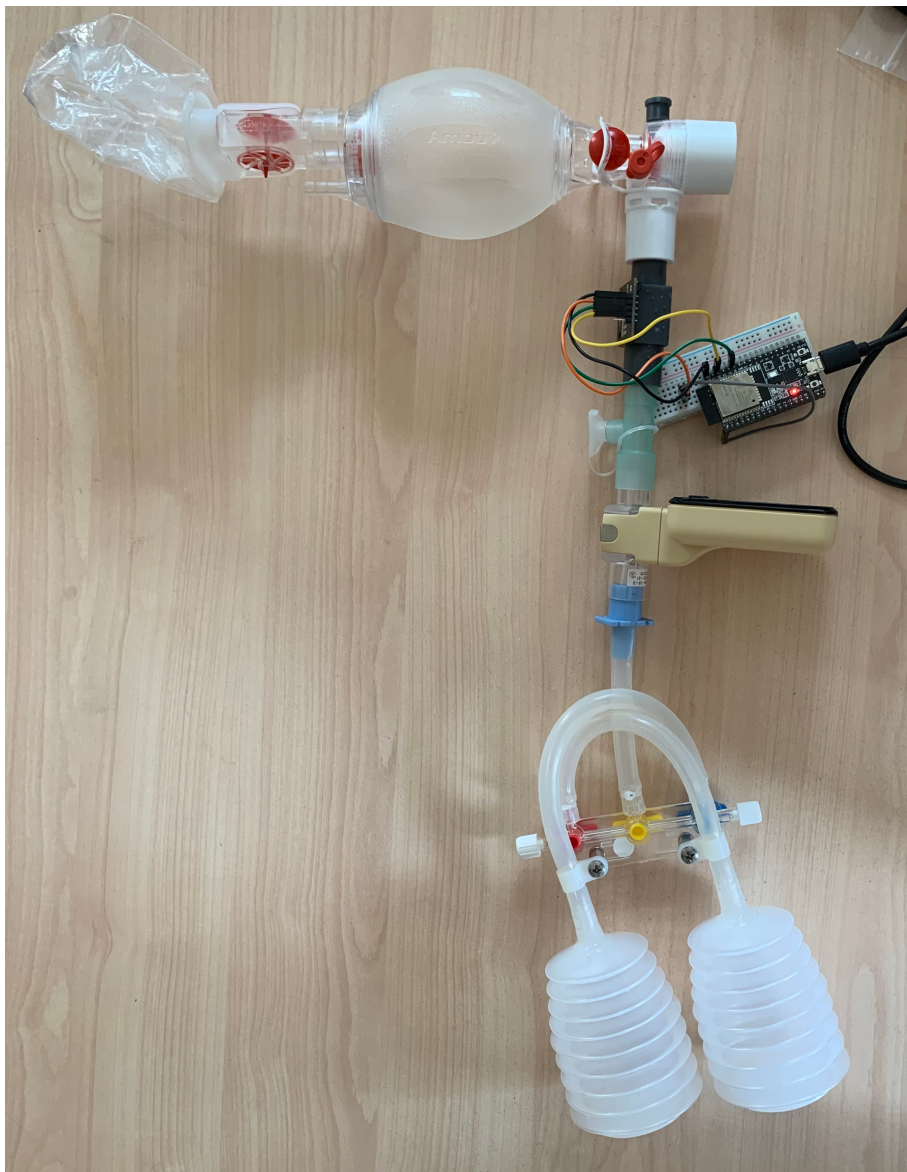


Figure A.4: Experimental Setup for Test 4.7.3